THE ASTROPHYSICAL JOURNAL, 494:453–471, 1998 February 10


# OPTICAL TOMOGRAPHY OF A SUNSPOT. I. COMPARISON BETWEEN TWO INVERSION TECHNIQUES

C. WESTENDORP PLAZA, J. C. DEL TORO INIESTA, B. RUIZ COBO, AND V. MARTÍNEZ PILLET
Instituto de Astrofísica de Canarias, E-38200, La Laguna, Tenerife, Spain[1]

AND

B. W. LITES AND A. SKUMANICH
High Altitude Observatory, National Center for Atmospheric Research,[2] Boulder, CO 80307[3]
*Received 1997 May 9; accepted 1997 September 22*

## ABSTRACT

A quantitative comparison between the Milne-Eddington (ME) inversion technique implemented by Skumanich & Lites and the SIR (Stokes Inversion based on Response Functions) proposed by Ruiz Cobo & del Toro Iniesta is presented. Numerical experiments are carried out to explore the capabilities and limitations of both diagnostic techniques. Such experiments consist of inversions of Stokes profiles previously synthesized in "realistic" solar atmospheric models. The results show that the ME inversion provides accurate, line-of-sight (LOS) averaged values for the input stratification of the vector magnetic field. Its greater speed compared to SIR makes it useful for quick analysis of large quantities of data (such as those currently provided by modern spectropolarimeters) if one is only interested in LOS-averaged quantities. However, the higher order description of the atmosphere used by SIR (which acknowledges variation of the thermal, dynamic, and magnetic parameters through the photosphere) allows retrieval of the stratification of all these parameters to good accuracy. This is so even in the presence of discontinuities such as those foreseen in magnetic canopies of sunspots. The trade-offs between thermodynamic and magnetic parameters observed in some ME inversions are reduced considerably in the case of SIR inversions because of the more realistic treatment of the thermodynamics in this analysis. Notably, both allow one to extract quantitative inferences of fairly weak magnetic fields (below 500 G), even when they are applied to Zeeman-sensitive lines in the visible spectrum; i.e., well below the commonly accepted limit of 500 G. The thermodynamic parameters resulting from the ME inversion are understood theoretically in terms of the generalized response functions introduced by Ruiz Cobo & del Toro Iniesta and through the concept of height of formation for inferred values proposed by Sánchez Almeida, Ruiz Cobo, & del Toro Iniesta.

The present comparison and verification of the reliability of inversion methods is a natural first step toward the ongoing analysis of the three-dimensional magnetic structure of a sunspot. By using SIR (with ME results for initialization) on maps of a whole sunspot observed by the Advanced Stokes Polarimeter, we obtain maps at different optical layers (i.e., an optical tomography) of the temperature, vector magnetic field, and LOS velocity. Such a tomography will appear in subsequent papers of the present series. To illustrate fits to the observed Stokes profiles, we show here actual inversion results for three points observed within a sunspot: one within the umbra, another from the outermost parts of the penumbra, and a third from the magnetic canopy surrounding the sunspot.

*Subject headings:* line: formation — radiative transfer — Sun: atmosphere — Sun: magnetic fields — sunspots

## 1. INTRODUCTION

This is the first paper of a series aimed at observational determination of the three-dimensional magnetic structure of a sunspot, motivated by new, detailed spectropolarimetric observations and by new analysis techniques that take advantage of the information contained in those observations. The new observational data have been provided by the Advanced Stokes Polarimeter (ASP, Elmore et al. 1992) in the form of bidimensional maps of line profiles of all four Stokes parameters (see Skumanich, Lites, & Martínez Pillet 1994 for a review). In principle, such information should allow one to infer the variation of physical parameters (vector magnetic field, temperature, velocities, etc.) along the line of sight (LOS) corresponding to each spatial point in the bidimensional map, thereby describing the three-dimensional structure (i.e., giving a "tomographic" analysis) of the sunspot within the range of physical height sampled by the observed photospheric spectral lines.

Although the observational information now available restricts us to a rather thin geometrical layer in the photosphere, many interesting processes are believed to take place within this volume, giving rise to a variety of structures, some examples of which are:

1. *Sunspot Umbrae.* The fine-scale structure of sunspot umbrae reveals bright "umbral dots" that suggest very small intrusions of hot, weakly magnetized, convecting plasma within the darker, strongly magnetized environs (Degenhardt & Lites 1993a, 1993b). Such structures are possible evidence for a very inhomogeneous subsurface field structure of sunspots, but conclusive evidence for weaker fields in umbral dots remains elusive, even though theory suggests that the nonmagnetic intrusions become considerably broader just below the layers for which most Zeeman-

[1] westend@iac.es, jti@iac.es, brc@iac.es, vmp@iac.es.
[2] The National Center for Atmospheric Research is sponsored by the National Science Foundation.
[3] lites@hao.ucar.edu, sku@hao.ucar.edu.

sensitive photospheric lines carry information. Given the extremely small size of umbral dots at the photosphere, the presence of such structures might be addressed more fruitfully at this point through an analysis of the *depth dependence* of the magnetic field rather than by pursuing an ultimate angular resolution.

2. *Sunspot Penumbrae.* Another region of the sunspot, the penumbra, has now been recognized to contain a very inhomogeneous vector magnetic field both horizontally and vertically. Unlike the umbra, the penumbra is known to have large gradients of magnetic field within the visible atmosphere. For example, one component of the outer penumbral field in the photosphere is nearly horizontal and evidently occupies a thin layer only one or two scale heights thick (Rimmele 1995a, 1995b; Stanchfield, Thomas, & Lites 1997; see also the review by Lites 1997). Evidence for such fine structure of the field is based on the behavior of observed Stokes $I$-profile asymmetries, but the observational picture remains incomplete at present. A tomographic analysis of these features based on inversion of the observed asymmetries of the full set of Stokes profiles may help to better define the physical state of sunspot penumbrae.

3. *Sunspot Canopies.* Finally, we cite as an example the "superpenumbral canopy" surrounding sunspots, where the magnetic field fills the volume outside the penumbra, but above the largely field-free photosphere (see, e.g., Lites 1997 and del Toro Iniesta 1997 for reviews). The canopy is likely to be an aspect of sunspots that is crucial to their structure and evolutionary history. As shown in this paper, parameters characterizing the canopy may be explored optimally with the aid of advanced techniques for analysis of detailed Stokes profiles.

Several recent observational studies have also indicated that variations with height of the vector magnetic field may exist in sunspots. Collados et al. (1994) inferred two model atmospheres of cool and hot umbrae that differ in variations of field strength with optical depth through the photosphere. Prior to that, Sánchez Almeida & Lites (1992) inferred from observations of the asymmetries of Stokes profiles in penumbrae that strong gradients of the vector magnetic field $\boldsymbol{B}$ may exist. Infrared observations also suggest a dependence with height of the field strength in penumbrae (Solanki, Rüedi, & Livingston 1992). Perhaps the clearest instance of large height gradients or discontinuities of $\boldsymbol{B}$ is the report of "superpenumbral canopies" in the photosphere surrounding sunspots: just beyond the outer penumbral boundary, one finds highly inclined magnetic fields above the visible photospheric surface (Solanki et al. 1992; Title et al. 1993; Lites et al. 1993; Adams et al. 1993; Zhang 1994; Solanki, Montavon, & Livingston 1994; Solanki, Finsterle, & Rüedi 1996). These results strongly suggest that surrounding the sunspot, the magnetic field overlies the quiet, nonmagnetic atmosphere. These recent inferences of superpenumbral canopies build upon the pioneering observations of canopy fields in the chromosphere by Giovanelli & Jones (1982). In this series of papers, we seek to establish a detailed, quantitative description of the height stratification of $\boldsymbol{B}$ through the photosphere *in* and *around* sunspots.

The availability of low-noise, accurate, full Stokes profile data from the ASP has provided considerable impetus for the development and utilization of more advanced Stokes profile inversion techniques. The information in the spectrally resolved Stokes profiles is much richer than that admitted by the Milne-Eddington atmospheric model, which forms the basis for routine analyses of ASP data. That technique, henceforth referred to as ME fitting, employs the Rachkovsky analytical solution (see Rachkovsky 1962, 1967) of the equations of polarized radiative transfer (RTE). In this model, the absorption matrix is constant along the LOS (hence the vector field $\boldsymbol{B}$); the component of velocity along the LOS $v$ and spectral line parameters, such as the line-to-continuum absorption coefficient ratio $\eta_0$, the Doppler width of the line $\Delta\lambda_D$, and the damping parameter $a$, are also constant. This computationally efficient method (see Skumanich & Lites 1987) permits one to process the large data sets produced by the ASP, but the results are inferences of $\boldsymbol{B}$ and other parameters that are effectively LOS averaged. In the absence of velocity gradients along the LOS, all four Stokes profiles exhibit definite symmetry properties (see Auer & Heasley 1978; Landi Degl'Innocenti & Landi Degl'Innocenti 1981). However, most Stokes profiles observed with the ASP show measurable asymmetries, even if such asymmetries are small in amplitude. Hence, the dynamics of the atmosphere in and around sunspots (including the most conspicuous manifestation, the Evershed effect) may not be represented correctly when analyses neglect the presence of velocity gradients. It is then clear that the ME fitting technique does not extract all the information encoded in the Stokes profiles (Sánchez Almeida & Lites 1992 and references therein). The observed asymmetries suggest that not only velocity gradients but also gradients along the LOS of the vector field and thermodynamic parameters are present and should be represented in the analysis. A more advanced inversion technique that allows for such gradients has the potential both to extract measures of those gradients and to provide a more meaningful interpretation of the LOS-averaged quantities resulting from ME fitting.

Recently developed inversion techniques (ITs), based on a more accurate representation of the physical state of the atmosphere than in the ME scheme, are able to utilize more of the information given by the spectrally and spatially resolved Stokes profiles. (For reviews of inversion of Stokes profiles, see del Toro Iniesta & Ruiz Cobo 1995, 1996, 1997.) A significant advance in the inference of atmospheric quantities is provided by the so-called SIR (Stokes inversion based on response functions; Ruiz Cobo & del Toro Iniesta 1992). Assuming LTE in a plane-parallel atmosphere, the SIR technique permits a variation of the atmospheric parameters along the LOS. For the most part, applications of SIR to real data have been restricted to analysis of Stokes $I$ and/or $V$ only, assuming hydrostatic equilibrium (e.g., del Toro Iniesta, Tarbell, & Ruiz Cobo 1994; Collados et al. 1994; Ruiz Cobo et al. 1996; Ruiz Cobo, Rodríguez Hidalgo, & Collados 1997). Except for a few restrictive cases (see del Toro Iniesta & Ruiz Cobo 1995, 1996) there have been no applications of this technique to observations of all four Stokes profiles. The ASP data then provide an excellent opportunity for embarking upon a *tomographic* analysis of a sunspot based on the SIR inversion. Such an analysis is the aim of this series of papers. Since the "natural" length scale for radiative transfer is optical depth, we shall first restrict the analysis to an optical tomography, i.e., to the inference of sunspot atmospheric parameters as a function of optical rather than geometrical depth (hence the

title of the series, Optical Tomography). Reference of the whole sunspot to a common geometric scale may become possible afterwards.

Before embarking upon an analysis of real data, it is crucial to understand the effectiveness and limitations of the diagnostic techniques. Information about the variation of atmospheric parameters along the LOS is encoded into the intensity and polarization of radiation (the Stokes profiles) emerging from the solar atmosphere. However, this encoding represents an integral along the LOS of functions, which depend nonlinearly on the parameters describing the solar atmosphere. Therefore, it is often difficult to isolate the influence on the emergent Stokes profiles of variations in any of the physical parameters. This frequently shows up in the ME inversion results as *trade-offs* between the parameters specifying the vector magnetic field and those specifying the thermodynamics. Such trade-offs are further amplified when the quality of the data is degraded from that usually obtained with the ASP; for example, when only one rather than two observed Zeeman-sensitive spectral lines are analyzed (cf. Lites, Martínez Pillet, & Skumanich 1994), or when the noise level of the observations is comparable to the polarization signals. Trade-offs also occur when the atmosphere departs significantly from the constant parameters of the Milne-Eddington model (Ruiz Cobo & del Toro Iniesta 1994). The influence of trade-offs depends on the ratio of Zeeman splitting, $\Delta\lambda_B$, to the Doppler width, $\Delta\lambda_D$: the weaker the field, the greater the chance of significant trade-offs. The reliability of ME fitting results has even been doubted in the weak field regime ($\Delta\lambda_B < \Delta\lambda_D$; see Lites et al. 1994), a matter that we address in detail in this paper. With an inversion technique such as SIR, we have the ability to greatly reduce this trade-off between the inferred thermodynamics and the magnetic field when LOS gradients are present.

The power and generality of high-order inversion methods raise questions as to the uniqueness and correctness of the numerous parameters needed to fully characterize the model atmosphere along the LOS. Furthermore, noise and systematic errors introduced by the measurement process may also compromise the inferred structure of the atmosphere. Thus, the focus of this first paper is to establish some expectations for the accuracy of physical parameters derived with both ME fitting and SIR. We compare the results of these two ITs as applied to synthetic profiles generated from several model atmospheres corresponding approximately to realistic solar scenarios with increasing degrees of complexity. That is to say, the various model atmospheres show different stratifications of the physical parameters from constant values up to significant *canopies*, quasi step functions of the logarithmic optical depth $\log \tau_5$ (throughout the paper we use continuum optical depths at 500 nm). Finally, we use the SIR inversion to make initial explorations of the LOS dependence of physical parameters of the atmosphere of a sunspot observed by the ASP. We apply the ITs to three points of the spot: the first is located in the umbra, the second in the outer penumbra, and the third in a region representing the immediate surroundings of the penumbra just beyond its visible boundary in the continuum.

The paper is structured as follows. First, in § 2 we explore the ability of the codes to recover magnetic field and velocity parameters without regard to their ability to discern the thermal properties of the atmospheres. The problem of disentangling trade-offs among thermodynamic, magnetic, and dynamic effects is considered in § 3. Inference of canopy-like magnetic structures is explored in § 4. In § 5 we apply the two techniques to Stokes profiles from ASP. Finally, in § 6 we summarize the main conclusions of this work.

## 2. SOUNDING THE MAGNETIC FIELD VECTOR AND THE LOS VELOCITY

In this section, we present a comparison of $\boldsymbol{B}$ and $v$ obtained with both ME and SIR inversions of Stokes profiles computed from three selected model atmospheres. The thermal structure of these atmospheres is taken from published models of actual solar features in order to test these inversion codes under conditions that they would likely encounter with real data. By knowing a priori the input atmosphere to the forward synthesis problem, we can accurately gauge the degree to which the ITs recover the magnetic and thermodynamic stratification we seek. We first apply the inversion to synthetic data generated with a constant vector magnetic field and LOS velocity. Next, we allow gradients of field and velocity in the models. We will demonstrate in this section that both codes work very well, recovering reasonable mean values for the field vector in the case of ME fitting, and quite satisfactory values of the input magnitudes and gradients in the case of SIR. We also demonstrate the influence of a nonmagnetic background, as in the case of stray light and/or a spatially unresolved magnetic structure, on the accuracy of these inversions.

We present results of numerical experiments using three standard thermal models: the umbral model E of Maltby et al. (1986; similar to the "cool" umbral model found by Collados et al. 1994), the penumbral model of del Toro Iniesta et al. (1994; similar to the "hot component" penumbral model of Kjeldseth-Moe & Maltby 1974), and the HSRA model (Gingerich et al. 1971). In all models, we adopt constant micro- and macroturbulent velocities of 0.6 and 0.75 km $s^{-1}$, respectively. The electron pressure is evaluated under the assumption of LTE ionization equilibrium and hydrostatic equilibrium. Since our ultimate aim is to apply the ITs to ASP observations of the well-known pair of Fe I lines at 630.15 and 630.25 nm, we compute synthetic Stokes profiles for both these lines, sampled every 1 pm, for the purpose of the tests reported here.

The SIR inversion method arrives at a solution through iterative perturbation of an initial guess as to the structure of the model atmosphere. The initial guess for the depth variation of a given physical parameter (the magnetic field strength, for example) may take on any variation of that parameter as a function of $\log \tau_5$. The perturbations applied to that initial guess by the SIR inversion at each iteration typically have a much more restricted possibility for variation with $\log \tau_5$. These perturbations are evaluated at a given number of discrete points, called nodes, along the LOS. The user of the SIR program may select the number of nodes to be perturbed for each parameter, the functional shape of the perturbation in between nodes being specified by a smooth interpolation. A single node forces the perturbation to that parameter to be constant with $\log \tau_5$ throughout the photosphere; specification of two nodes allows a linear perturbation with $\log \tau_5$ of that parameter; three nodes allow a second-order perturbation. For more than three nodes, the perturbation is specified by standard splines (i.e., splines without tension) of the corresponding order. Practice reveals that the optimum solution is reached

by steadily increasing the degree of complexity of perturbations (i.e., the number of nodes) from one iteration to the next until no significant improvement of the fit profiles is obtained. A particular inversion may be characterized for simplicity by an order equal to the final number of nodes for each parameter.

Unless otherwise stated, all tests presented in this paper use a final five nodes for temperature and one node for micro- and macroturbulence (turbulence is assumed to be constant with depth). We have chosen three different runs to illustrate the results from the SIR inversion; these are referred to as SIR + 1, SIR + 2, and SIR + 5. SIR + 1 uses a final one node for $\boldsymbol{B}$ and $v$, and SIR + 2 a final two nodes. SIR + 5 uses a final five nodes: three for LOS velocity, magnetic field strength and inclination, and two for azimuth. Note that accurate, synthetic Stokes profiles from a full radiative transfer (LTE) code require a much finer sampling with optical depth than would be possible from a representation of the variation at only a few nodes. Typically, 25 points are used[4] in SIR to allow accurate computation of the formal solution to the equations of polarized radiative transfer through the photosphere.

### 2.1. *Constant Magnetic Field and LOS Velocity*

We begin with a presentation of our results for the inversion of synthetic Stokes profiles generated with a constant vector magnetic field $\boldsymbol{B}$ and LOS velocity $v$. This allows us to gauge the improvement of the results of SIR over ME fitting. Note that while SIR accounts for (five-node) modification of the temperature stratification (of *any* initial functional shape), ME fitting uses a Milne-Eddington atmosphere (linear shape of the source function with optical depth and constant $\Delta\lambda_D$, $a$, and $\eta_0$). We perform tests for a range of magnetic field strengths and angles in order to explore doubts that have been raised about the minimum magnetic field strength for which these ITs yield reliable results (Lites et al. 1994).

We have built a grid of 1920 models with the three temperature models cited above, with ten different values of the constant field strength ($B$ = 50, 100, 150, 200, 300, 500, 750, 1000, 1500, and 2000 G), four different values of the magnetic inclination with respect to the line of sight ($\psi = 5°$, 20°, 60°, and 90°), four values of the magnetic azimuth ($\phi = 0°$, 20°, 80°, and 120°), and four values of the LOS velocity ($v$ = 0, 0.1, 0.5, and 1 km s$^{-1}$). To the synthetic Stokes profiles from these models we add a normally distributed (pseudo) random noise, in order to simulate profiles measured by real instruments where the S/N ratio is often an overriding limitation to the accuracy of the inversion results. We choose three different S/N ratios for the continuum intensity: S/N = 100, 200, and 1000, with the latter being typical for ASP data outside of sunspot umbrae. By carrying out the inversions on data with 18 statistical realizations of the S/N, we may estimate the mean value and errors introduced by each noise level. More than $10^5$ inversions have been carried out with both the ME fitting and the SIR + 1 codes.

We examine the difference between output (solution) and input (synthetic) values of the physical quantities ($\Delta B$, $\Delta\psi$, $\Delta\phi$, and $\Delta v$). The statistical distributions and mean values of these differences are similar for all three chosen models of temperature stratification. In Figures 1 and 2 we display mean (over 18 realizations of noise) differences and rms fluctuations of the quantities describing $\boldsymbol{B}$, as a function of assumed field strength $B$, for the umbral model with $\psi = 60°$ and $\phi = 80°$, and for three different values of the S/N. Plots of $\Delta v$ are not shown, because the LOS velocity was accurately recovered in all cases by both ME fitting and SIR, with differences typically less than 40 ms$^{-1}$. As anticipated from examination of the fits to the profiles, both inversion methods cope well with noise: the larger the S/N ratio, the smaller the rms error of the recovered parameters. Henceforth, we will only use S/N = 1000 in the numerical experiments, as representative of ASP observations, unless otherwise stated.

It should be noted that the ME technique, in spite of its low-order representation of the thermodynamics, provides reliable results for constant magnetic field strengths as small as 100 G. This strength is well below the threshold foreseen by Lites et al. (1994). For the assumed field strength of 100 G (and unit filling factor), $\Delta B < 25$ G (rms) and $\Delta\psi$, $\Delta\phi \lesssim 6°$ (rms). These rms errors are $\lesssim 70$ G and $\lesssim 0.^\circ 2$ when the field strength increases to 1000 G. The SIR + 1 results are $\Delta B < 30$ G and $\Delta\psi$, $\Delta\phi \lesssim 2°$–3° for $B = 100$ G, and $\Delta B <$ 10–20 G and $\Delta\psi$, $\Delta\phi \lesssim 0.^\circ 2$ for $B > 500$ G. *Hence, the general belief that lines in the visible spectrum do not allow estimates of fields weaker than around 500 G is not well founded.* The reasoning behind this erroneous conjecture is that Stokes profiles for Zeeman splitting of less than 1 Doppler width are believed to obey the so-called weak-field approximation, in which Stokes $V$ is proportional to the derivative of Stokes $I$ (see Jefferies, Lites, & Skumanich 1989 for an exposition of the weak-field approximation for all Stokes parameters). This approximation is only first order, but ME fitting and, of course, SIR account for transfer effects that go well beyond this first-order approximation. To the extent that the measured profiles resolve the higher order variations in the profile shapes, the inversion techniques should be sensitive to fields much weaker than the weak-field criterion (about 600 G for Fe I 630.25 nm). This sensitivity is, of course, highly dependent upon the availability of spectrally resolved Stokes profiles with excellent S/N. The effective S/N is decreased if the filling factor is less than unity; therefore, the inference of accurate field strengths is less precise than predicted by the simulations given here (see § 2.2).

The noticeable dip in the lower left panel of Figure 1 runs counter to expectation, i.e., for larger input field strengths, the absolute relative error $|\Delta B/B|$ decreases. Similar dips are not present in any of the other computed magnetic configurations. This local maximum of $|\Delta B/B|$ around 1300 G suggests a trade-off between the inferred thermodynamic and magnetic parameters. A more detailed analysis is deferred to § 3.

### 2.2. *Stray Light and/or Lack of Spatial Resolution*

Both ME and SIR inversion methods allow one to infer a filling factor for the magnetized component within each spatial resolution element in order to account for a spatially unresolved magnetic structure in a nonmagnetic environment and/or scattered light. Both codes assume that a fraction $1 - f$ of a nonmagnetic profile (Stokes $I$ only) adds to the profiles (scaled by a factor $f$) from the magnetic regions.

[4] Perturbations of the physical parameters at points other than the nodes are assumed to follow the cited splines. See details in Ruiz Cobo & del Toro Iniesta (1992).

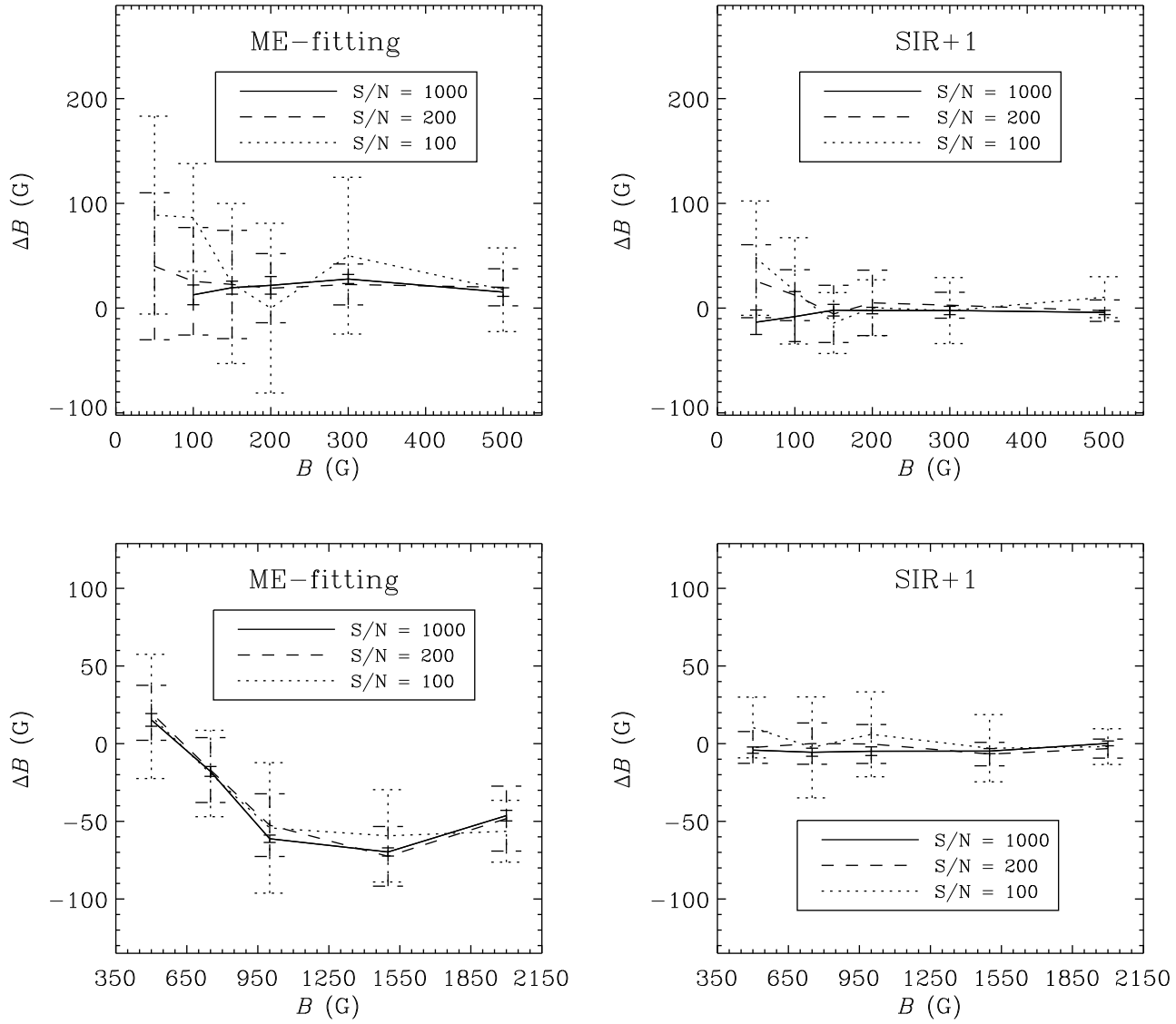


FIG. 1.—Field strength errors $\Delta B$ (inversion fit, synthetic model) for the constant field case with $\psi = 60°$ and $\phi = 80°$ are shown for ME fitting (*left*) and SIR + 1 (*right*) as a function of the synthetic model field strength for the umbral temperature stratification. Line types represent different values of S/N. Error bars show rms fluctuations from a sample of 18 inversions with different realizations of the (pseudo) random noise.

As noted above, the dilution of the polarization signal mimics observations of reduced S/N, but the observed Stokes $I$-profile may differ substantially from the case $f = 1$. Some tests of the ME inversion on "unresolved" synthetic flux tube data have already been carried out (Skumanich, Grossmann-Doerth, & Lites 1992), with results that recovered the approximate size and field magnitude of the flux tube. (More sophisticated ITs are also available; see Bellot Rubio, Ruiz Cobo, & Collados 1997.)

Here we confirm that both the ME and SIR inversions give accurate filling factors when applied to several of the cases described in § 2.1. The stray-light unmagnetized (zero-velocity) profile used in the following calculations has been synthesized with the quiet Sun thermal model. Provided that the field strength is larger than 500 G, inversions for cases with $f = 0.05$, 0.1, and 0.2 met with excellent results. In all modes tested, both ME and SIR inversions retrieve $f$ with an accuracy better than 5% and with errors in the remaining parameters similar to those reported in § 2.1. At lower field strengths, the smaller the filling factor, the lager the error. In fact, longitudinal fields of $B < 200$ G and $f < 0.1$ and transversal fields of $B < 300$ G and $f < 0.1$ produce polarization signals (integrated over the line profile) that fall below the standard (but conservative) threshold used by ASP to reject profiles with signals insufficient for an accurate inversion ($4 \times 10^{-3} I_c$). We have used the present simulations to estimate the minimum (reasonably) detectable field strength under the least favorable thermodynamic conditions: when both the magnetic and the nonmagnetic atmosphere have the same temperature structure (here assumed to be that of the quiet Sun). The results are displayed in Table 1.

In order to understand why these reasonable estimates can be obtained from visible lines, consider following analytical reasoning. Let us call $R(\lambda)$ the residual of a first-order expansion[5] of the purely magnetic $V$-profile, $V_{\rm mag}$, on $B$, i.e.,

$$R(\lambda) = V_{\rm mag}(\lambda) - \frac{\partial V_{\rm mag}(\lambda)}{\partial B} B \, . \quad (1)$$

[5] Note that the weak-field approximation implies such a linearity between $V_{\rm mag}$ and $B$.

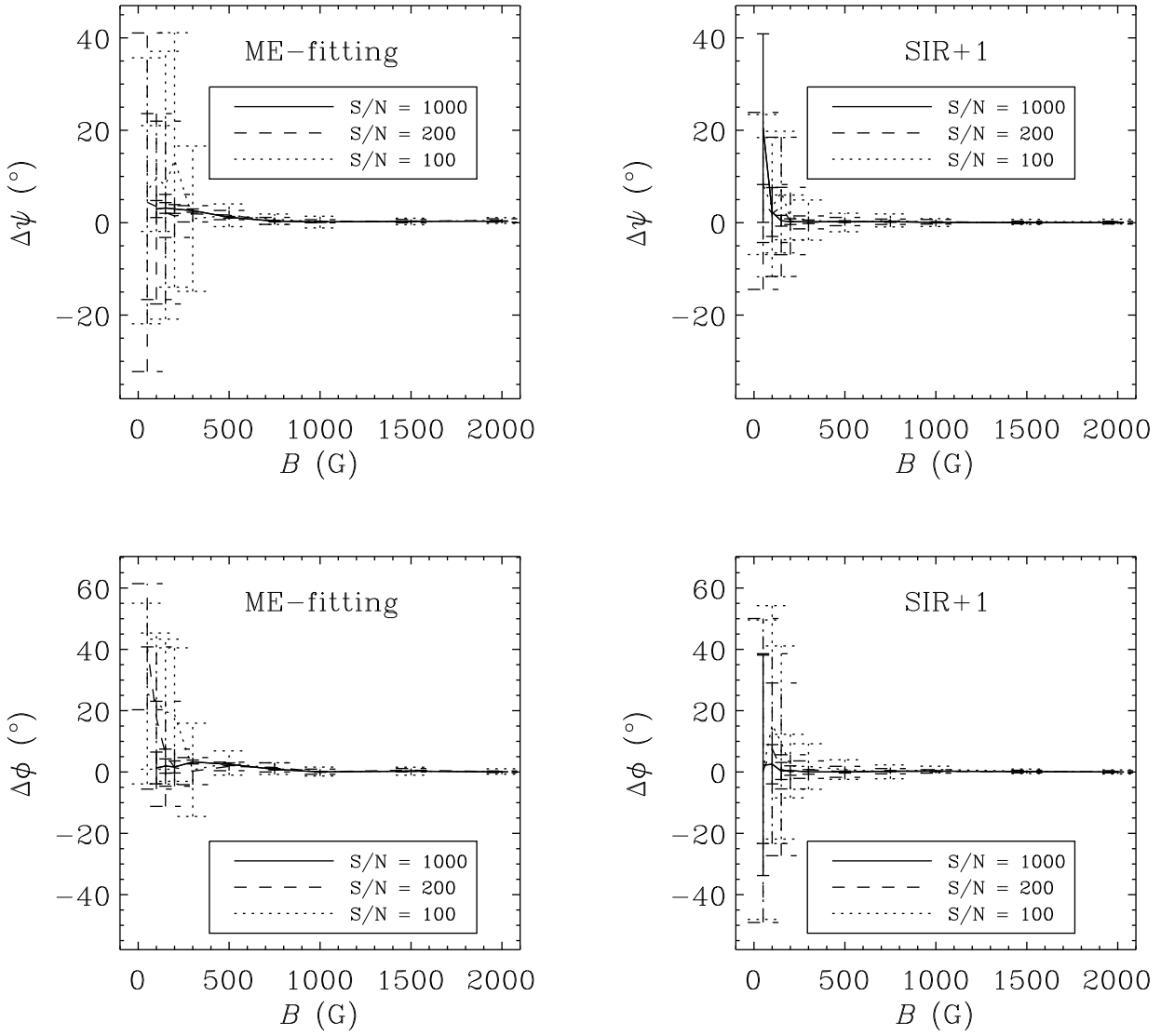


FIG. 2.—Same as Fig. 1, but showing the differences of magnetic inclination $\Delta\psi$ and azimuth $\Delta\phi$

Note that $R(\lambda)$ contains higher-order terms of $V_{\rm mag}$ on $B$.

The observed $V$-profile can thus be expressed as

$$V_{\rm obs} = fB\,\frac{\partial V_{\rm mag}(\lambda)}{\partial B} + fR(\lambda) + N(\lambda)\,, \qquad (2)$$

TABLE 1

MINIMUM DETECTABLE UNRESOLVED WEAK FIELDS

| | OUTPUT | |
|---|---|---|
| INPUT | ME | SIR+1 |
| $B$ 200 ..... | 340 ± 100 | 310 ± 110 |
| $f$ 0.2 ..... | 0.14 ± 0.04 | 0.16 ± 0.06 |
| $\psi$ 0 ..... | 17 ± 8 | 18 ± 6 |
| $\phi$ undetermined..... | 40 ± 25 | 60 ± 50 |
| $B$ 300 ..... | 470 ± 70 | 390 ± 80 |
| $f$ 0.3 ..... | 0.15 ± 0.04 | 0.21 ± 0.08 |
| $\psi$ 90..... | 90.1 ± 0.6 | 90.1 ± 0.5 |
| $\phi$ 0 ..... | 20 ± 10 | 0 ± 1 |

NOTE.—. Field strength in given in G, angular quantities in degrees. Uncertainties are rms values after inversion with the 18 realizations of noise.

where $N(\lambda)$ stands for the noise of the data. If $fR(\lambda)$ is well above $N(\lambda)$, then deviations from linearity can be reasonably detected. In other words, should $1/(fR)$ be less than $1/N$ ($1/N$ since all profiles are normalized to the continuum), we can expect to retrieve good estimates of $B$. In Figure 3, we plot $1/(fR)$ (at the wavelength of the positive $V$-peak) versus $B$ for two values of the macroturbulence, 0 km s$^{-1}$ (*solid lines*) and 0.75 km s$^{-1}$ (*dashed lines*). The thermodynamics is again that of the quiet Sun. Note that for $\xi_{\rm mac} = 0$, $B = 200$ G (longitudinal), and $f = 0.2$, $1/(fR) < 10^3$ (the S/N of the sample profiles, indicated by a dotted line). Of course, a higher macroturbulence imposes higher constraints, but remember that macroturbulence is nothing but an ad hoc parameter to further account for a lack of spatial resolution. The results reported here give us confidence that the weak internetwork fields observed with the ASP (Lites et al. 1996) are large enough to state that they are well below 1000 G in strength.

From these results, we conclude that an enhancement of the spatial resolution of the Stokes profile observations in the visible spectrum with a consequent increase in filling factor, or observations in the infrared where the magnetic

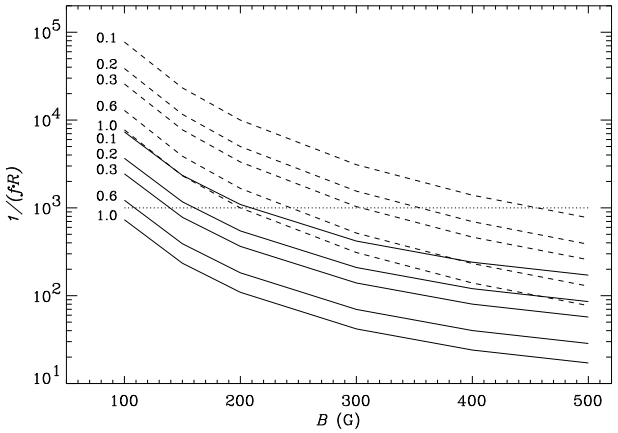


FIG. 3.—Parameter $1/(fR)$ versus field strength. *Solid lines*: $\xi_{mac} = 0$ km $s^{-1}$, *dashed lines*: $\xi_{mac} = 0.75$ km $s^{-1}$. Labels correspond to different filling factors. See text for details.

splitting is greater, are both worthwhile endeavors. In any event, spectral lines in the visible can give reasonable estimates of the magnetic field vector for weak fields, either resolved or moderately unresolved.

### 2.3. *Variable Magnetic Field and LOS Velocity*

Here we explore the inversion of Stokes profiles synthesized from atmospheres in which the magnetic field and velocity may vary along the LOS. Ruiz Cobo & del Toro Iniesta (1994) and del Toro Iniesta & Ruiz Cobo (1996) demonstrated the importance of permitting LOS gradients of physical quantities when analyzing spectropolarimetric observations. Therefore, we anticipate that the SIR technique will be able to exploit more of the information present in the Stokes profiles than will the ME inversion. Analysis techniques for spectral data will be sensitive to conditions at different heights in the atmosphere, depending upon the model stratification (Sánchez Almeida et al. 1996). These issues are of particular concern for both ME fitting and SIR + 1, as the two methods assume that $\boldsymbol{B}$ and $v$ are constant throughout the photosphere. Here, we estimate the limitations imposed by these two techniques and their assumptions on the interpretation of Stokes profiles formed in atmospheres with variable magnetic fields and LOS velocities. We also investigate the extent to which higher order inversions, such as SIR + 2 and SIR + 5, improve the results.

The first set of five numerical experiments we present have field strengths that vary nonlinearly with $\log \tau_5$ between 1000 and 2500 G (*solid lines*, *top left panels*, Figs. 5, 6, 7, and 8), with five different variations of $\psi$ versus $\log \tau_5$ (*solid lines*, *lower left panels*, Figs. 5, 6, 7, and 8). We assume a null LOS velocity and a constant $\phi = 0°$. Rather than listing the inferred values $B_i$, $\psi_i$, and $\phi_i$ as recovered by ME fitting and SIR + 1 for all three thermal models, we show in Figure 4 the optical depths $\tau_i$ at which the inversion results replicate the model values, i.e., $B_i = B(\tau_i)$ or $\psi_i = \psi(\tau_i)$. Indicated on the abscissa of this plot are the ranges of $\psi$ corresponding to each of the five selected models for this parameter. Because the input models have $\phi = \text{const}$, no $\tau_i$ can be specified for this quantity, but errors in $\phi$ do not exceed 4°–5° in the worst case where $0° < \psi < 20°$ (the Stokes $Q$- and $U$-profiles are smaller than the noise in this

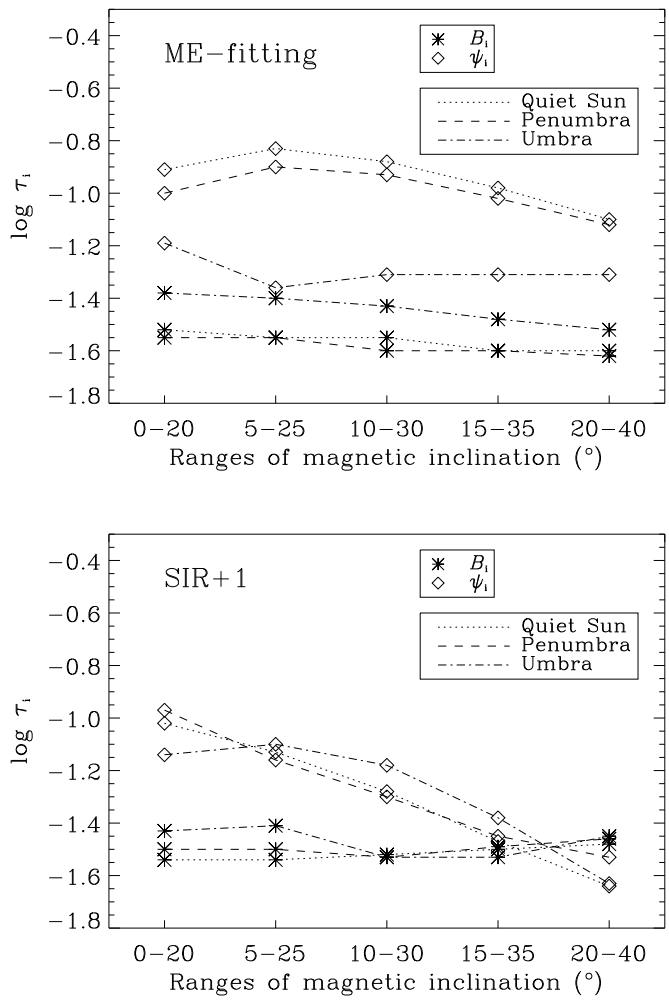


FIG. 4.—Optical depths ($\log \tau_i$) at which inferred parameters ($B_i$, $\psi_i$) replicate a value of the "real" stratification [$B(\tau_5)$, $\psi_0(\tau_5)$; see plots in Fig. 5].

case). According to Sánchez Almeida et al. (1996), for any given thermal stratification, $B_i$ and $\psi_i$ may represent the field at distinctly different optical depths. In the examples of Figure 4, this difference can be as large as 0.8 dex (roughly 80 km in geometrical height). From this figure, we note that $\psi_i$ tends to bring information for deeper layers than $B_i$. Moreover, this separation in $\tau_i$ for $B_i$ and $\psi_i$ depends on the chosen model atmosphere (quiet Sun, umbra, or penumbra) or the inversion technique (ME fitting or SIR + 1).

Figures 5 and 6 illustrate the results of SIR + 2 and SIR + 5 as applied to Stokes profiles synthesized from the umbral model. Permitting the inversion method to allow for LOS variations greatly enriches the information content of the result. *The improvement of the SIR + 5 results over those of SIR + 2 indicates that information about these higher order variations is indeed contained within the synthetic Stokes profiles.*

We now consider the introduction of a velocity gradient in our five cases. Our results for SIR + 2 and SIR + 5 using the umbral model are illustrated in Figures 7 and 8. It is apparent that velocity is well recovered. In addition, there is improvement in the fit to the other parameters. *The appearance of asymmetries in the Stokes profiles decrease the inherent redundancy of the data: in the absence of velocity*

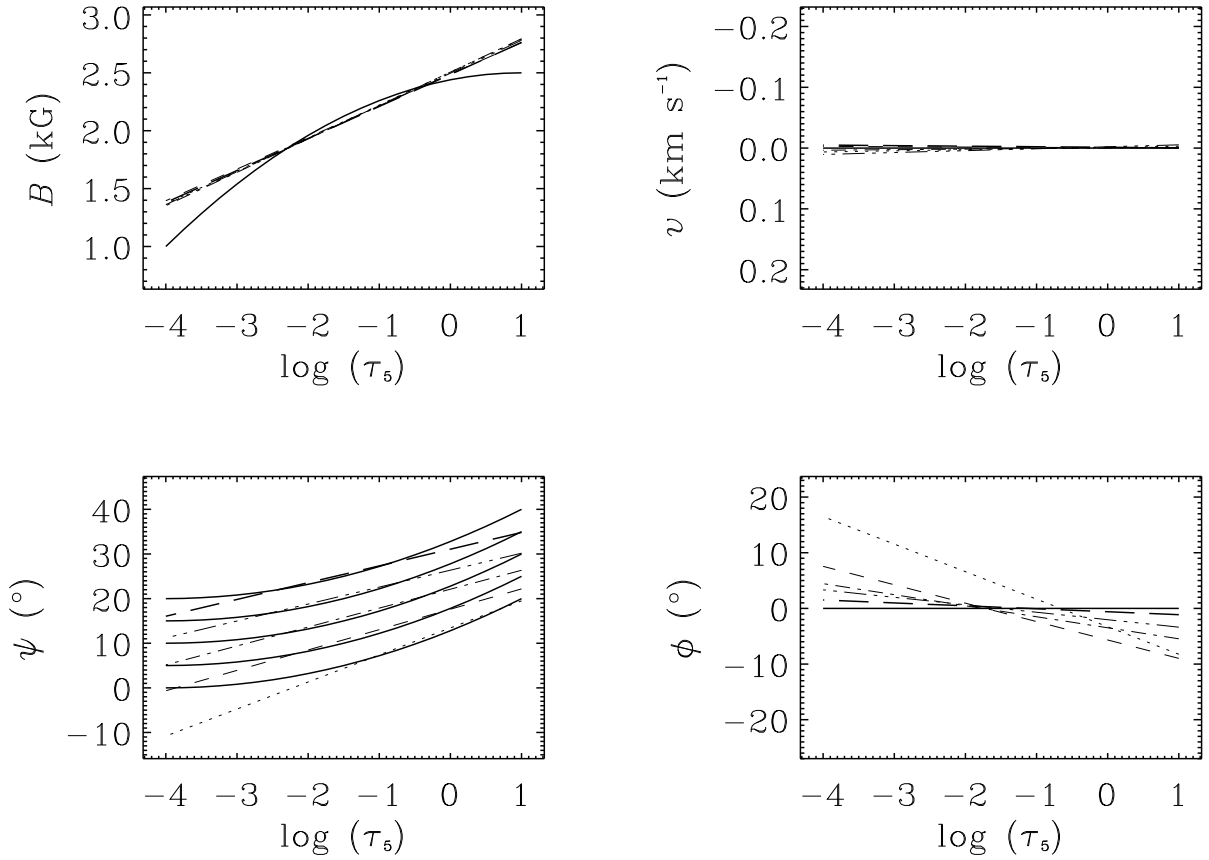


FIG. 5.—Results of the inversion with SIR + 2 for profiles synthesized for five field inclinations (*solid lines*), each with a higher offset of the inclination: offsets are $\psi = 0°$ (*dotted lines*), $\psi = 5°$ (*dashed lines*), $\psi = 10°$ (*dash-dotted lines*), $\psi = 15°$ (*dash-triple-dotted lines*), and $\psi = 20°$ (*long-dashed lines*); the range is 20°.

*gradients, wavelength samples symmetric with respect to line center carry identical information.* These results lend credibility to the extraction of gradients, and even the curvature with optical depth, of the magnetic field and the LOS velocity. Such an enhancement of the diagnostic capabilities as a result of the presence of velocity variations has been demonstrated previously by del Toro Iniesta & Ruiz Cobo (1996).

The azimuth $\phi$ is constant throughout all of the models tested in Figures 5–8, but the fit to $\phi$ is allowed to vary. Larger departures of the azimuth from the input values are to be expected when $\psi(\tau_5)$ is small, since the Stokes $Q$- and $U$-profiles are small in amplitude and may be dominated by noise. In SIR inversions, it may be desirable to constrain the field azimuth to be constant when the inversion approaches small values of $\psi(\tau_5)$ (i.e., to select the number of nodes for $\phi$ to 1). In the application of SIR to real data, we have found it necessary to adjust the number of nodes for some of the physical quantities. Since in real observations the input model (the solar model) is unknown, the quality of the fit to the profiles is the only criterion used to adjust the number of nodes.[6] A version of the SIR code that automatically selects the number of nodes for the different atmospheric quantities is being planned for the near future. Until this is done, manual adjustment will be necessary to gain more precise insight into the depth dependence of the vector magnetic field.

[6] This adjustment is a sequential increase of the number of nodes until no significant improvement of the fit to the profiles is reached; see § 2.

## 3. TRADE-OFFS AMONG LINE FORMATION PARAMETERS AND THE VECTOR FIELD IN A FULLY VARIABLE ATMOSPHERE

The results presented above for our model atmospheres with variable vector magnetic field and LOS velocity indicate that if we are satisfied with some LOS-averaged measure of $\boldsymbol{B}$ and $v$ and not interested in temperatures, ME fitting is a wise choice for an inversion technique. This is so not only because of the computational efficiency of the method, but also because the results are very representative of the mean of each quantity and differ only slightly from the results of SIR + 1, where the stratification of temperature and line formation parameters $\Delta\lambda_D$, $a$, and $\eta_0$ are much more realistic. The slight dependence of ME values with the thermal stratification reported in § 2 suggests that ME fitting may effect a trade-off among the free parameters. This trade-off compensates for the model's inability to reproduce the depth variation of certain line formation parameters. For example, atmospheric models for the quiet Sun have a dramatic variation of the line-to-continuum opacity ratio $\eta_0$ of the Fe I 630 nm lines within the photosphere. This variation is not represented by the ME inversion, as we show here. Another example is the dip in the curves of the lower left panel of Figure 1, which disappears for higher values of the microturbulence of the input model atmosphere, thereby increasing the Doppler width of the lines. Yet another example is presented in Figure 9, where different inferred values of $\Delta\lambda_{D,i}$, $\eta_{0,i}$, and $a_i$ are displayed for input model atmospheres differing only in the magnetic

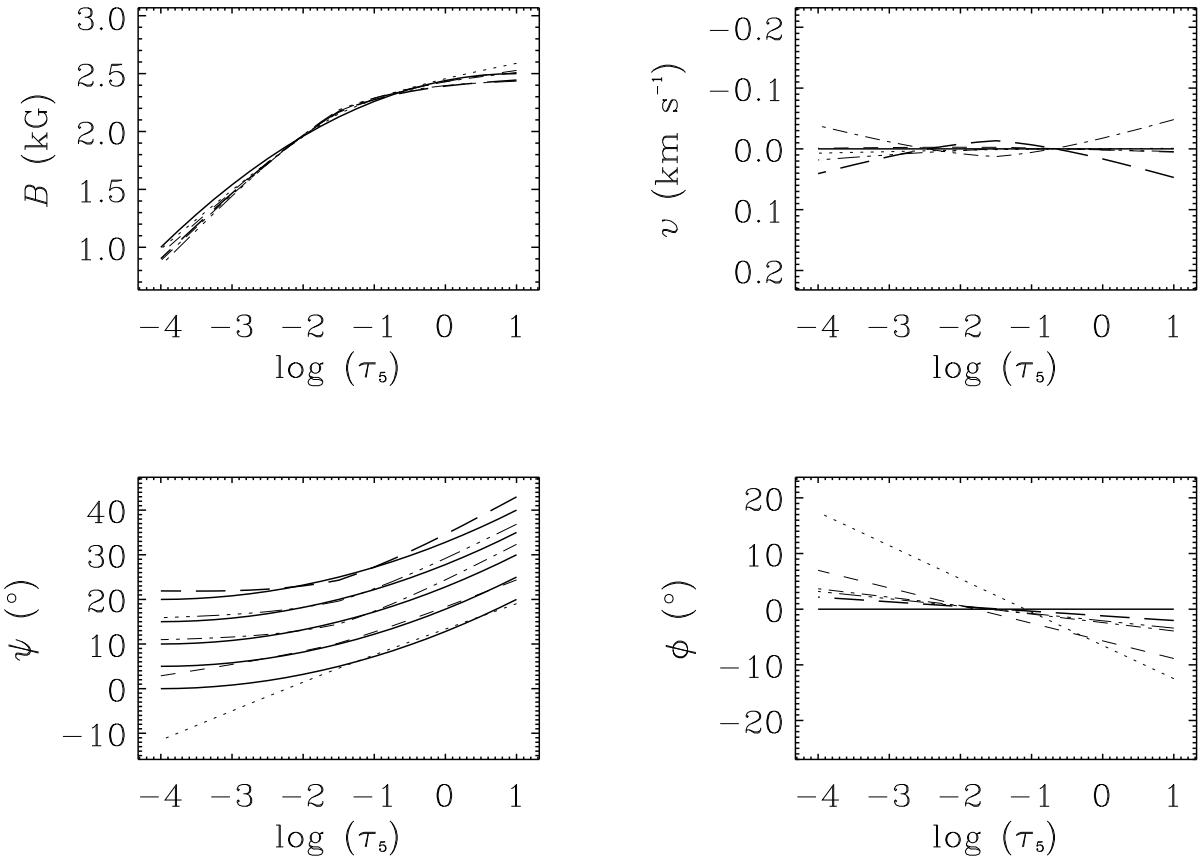


FIG. 6.—Same as Fig. 5, for SIR + 5

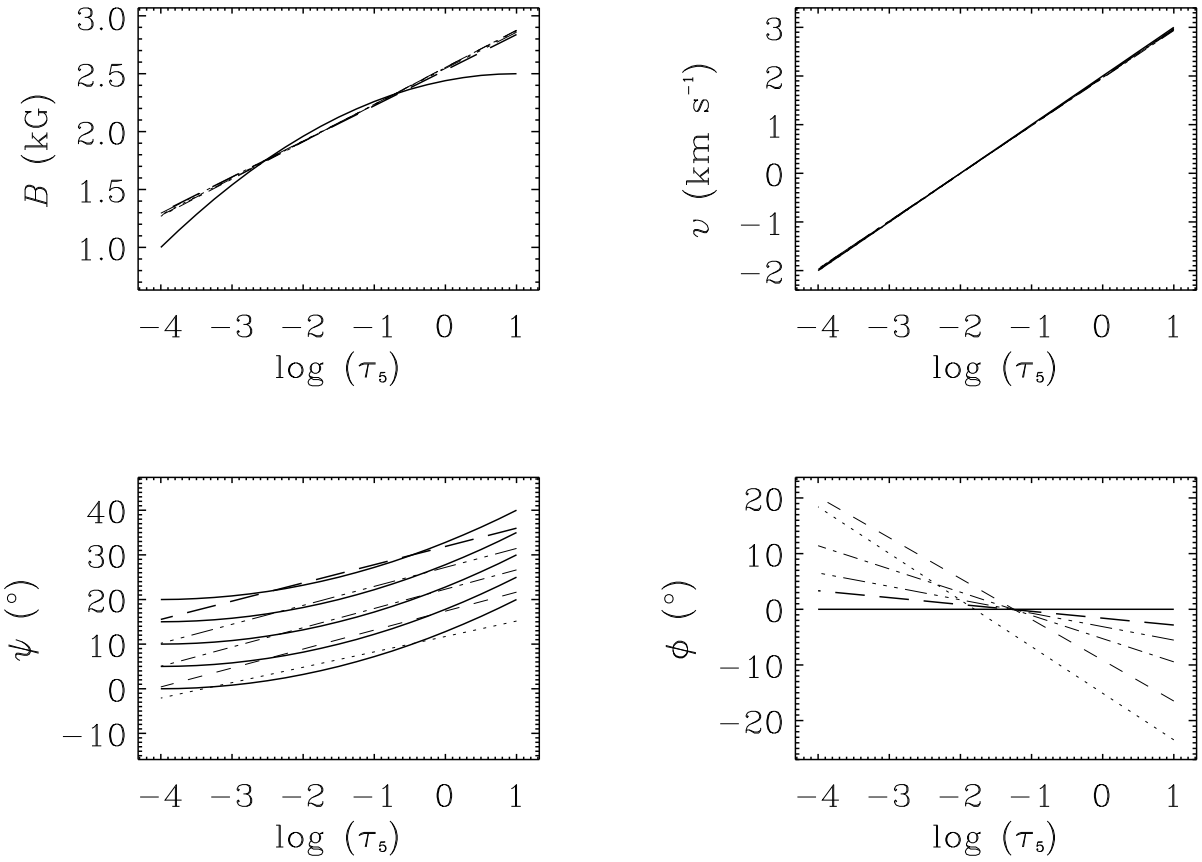


FIG. 7.—Same as Fig. 5, but with a gradient in LOS velocity

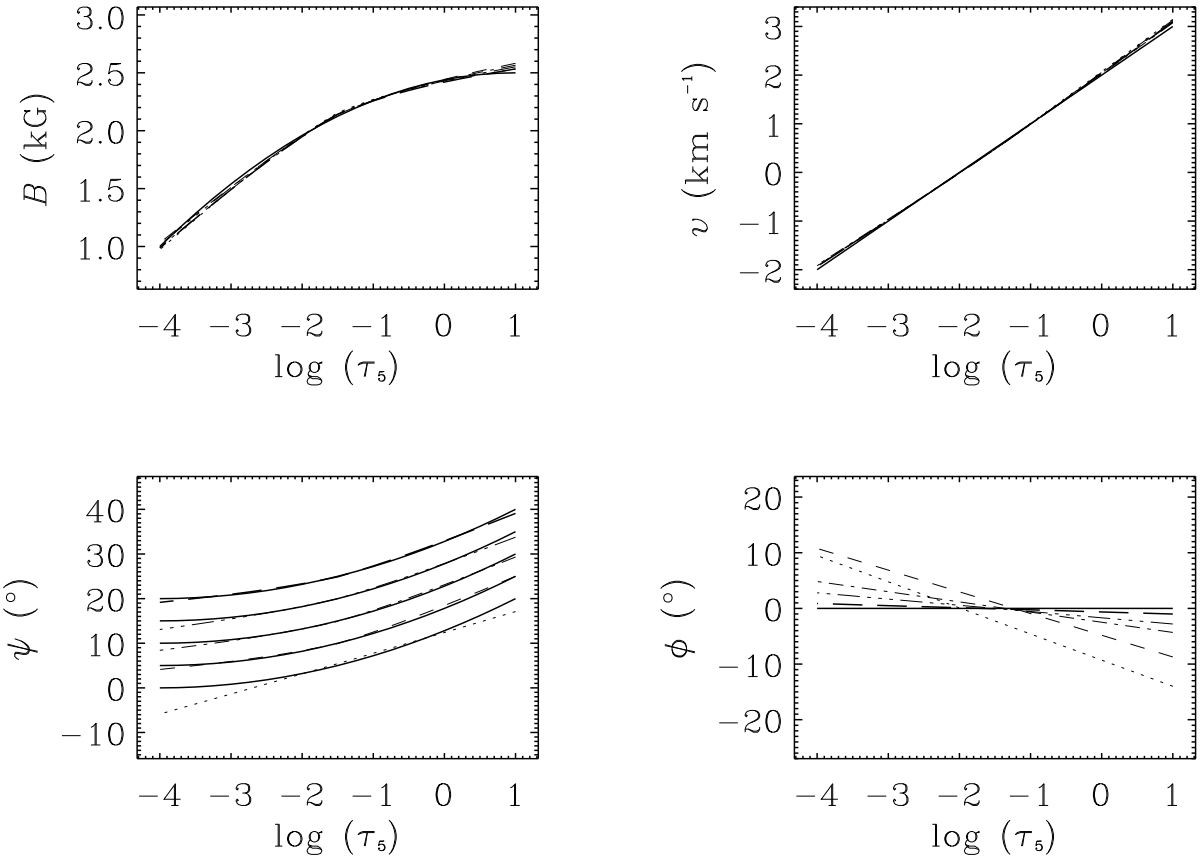


FIG. 8.—Same as Fig. 7, for SIR + 5

field strength (temperatures of this example correspond to the quiet Sun model). If no coupling between thermodynamic and magnetic parameters were present, no variations in the output values of these parameters would be apparent. Note also that the inferred opacity ratio $\eta_0$ represents values of the input stratification at layers deeper than log $\tau_5 = -0.5$. We examine the origin of this in § 3.1.

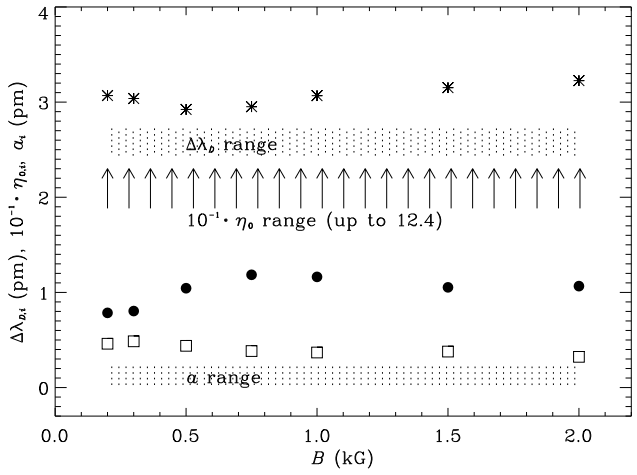


FIG. 9.—Results from ME fitting (thermal quiet-Sun model, macroturbulence of 0.75 km s$^{-1}$, and $S/N = 1000$), showing Doppler width (*asterisks*), line-to-continuum ratio of absorption coefficients (*filled circles*), and damping parameter (*squares*) as a function of the *constant* magnetic field strength. Shaded areas indicate the values over which the synthetic $\Delta\lambda_D$ and $a$ range throughout the photosphere (log $\tau_5 \in [-2.5, -0.5]$). The dimensionless $\eta_0$ ranges from the bottom of the arrows up to 12.4.

The trade-offs among the different thermodynamic parameters (and to a lesser extent, between magnetic field and thermodynamic parameters) can be traced to the inability of the Milne-Eddington approximation to account for variations through the photosphere. First, the temperature variation represented by the Milne-Eddington parameters $B_0$ and $B_1$ frequently cannot represent the actual temperature stratification. This is illustrated in Figure 10, where we plot differences between the input and output (from ME

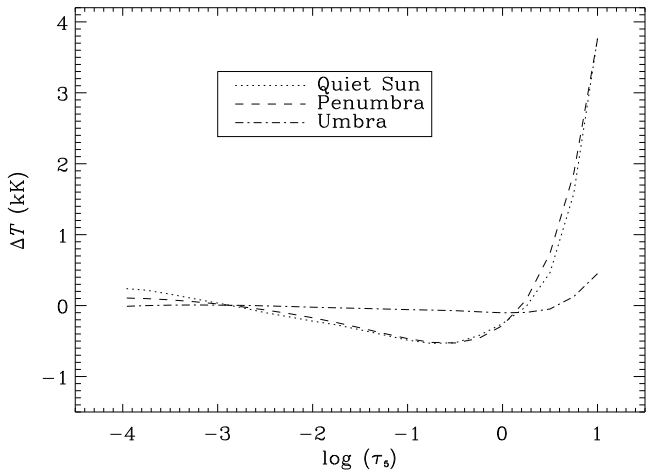


FIG. 10.—Difference in temperature between output (ME fitting) and input models for the quiet-Sun, penumbral, and umbral atmospheres. Examples are taken from inversions of the profiles shown in Fig. 5 (with an inclination offset of 20°).

TABLE 2

RESULTS FROM ME FITTING FOR STOKES PROFILES SYNTHESIZED IN THE UMBRAL MODEL

| Mode | $B_i$ | $\psi_i$ | $\phi_i$ | $\Delta\lambda_{D,m}$ | $a_i$ | $\eta_{0,i}$ | $B/I_c$ | $B_1/I_c$ | $\chi^2$ |
|---|---|---|---|---|---|---|---|---|---|
| | | | | $B = 1000$ G | | | | | |
| a..... | 938.8 | 60.1 | 79.9 | 24.9 | 0.27 | 31.8 | 0.096 | 0.129 | $3.2 \times 10^{-3}$ |
| b..... | 1000.0* | 60.0* | 80.0* | 23.5 | 0.26 | 36.7 | 0.100 | 0.123 | $3.9 \times 10^{-3}$ |
| | | | | $B = 500$ G | | | | | |
| a..... | 514.0 | 61.4 | 82.4 | 23.1 | 0.32 | 29.6 | 0.099 | 0.125 | $3.2 \times 10^{-3}$ |
| b..... | 500.0* | 60.0* | 80.0* | 23.1 | 0.29 | 32.6 | 0.101 | 0.125 | $3.9 \times 10^{-3}$ |

Model with two values of the input field strength (1000 and 500 G) and two inversion modes. (*a*) Normal mode; (*b*) after fixing $B$, $\psi$, and $\phi$ (numbers indicated by asterisks) to the input value.

fitting) temperature stratification for the three model atmospheres (quiet Sun, umbra, and penumbra). The retrieved umbral temperature stratification is a reasonable representation of the input model. Indeed, when plotted against $\tau_5$, the (LTE) source function computed for model E of Maltby et al. (1986) closely resembles a straight line from $\log \tau_5 = 0.5$ upward. This is by no means the case for the quiet and penumbral models, which show $\Delta T \in [500, 1000]$ throughout the photosphere. The remaining thermodynamic free parameters of ME, $\eta_0$, $\Delta\lambda_D$, and $a$, vary with depth in "real" atmospheres, as depicted in Figure 9, where the range of values for $\log \tau_5 \in [-2.5, -0.5]$ are displayed. Therefore, although simple and helpful, the Milne-Eddington approach introduces some unavoidable trade-offs among its parameters.

As the intrinsic errors in the thermodynamic parameters of the ME inversion may be compensated for, to some extent, by errors in the inferred magnetic parameters in order to improve the overall fit to the Stokes profiles, we examine the magnitude of such errors as described in what follows. In numerical experiments similar to those carried out by Lites & Skumanich (1988) for exploring inversions of the chromospheric Stokes profiles of the Mg I $B$ lines, we have inverted the synthetic Fe I lines using two modes: the usual mode in which all the parameters are free and a mode in which the *constant* vector magnetic field is kept fixed to the "real" value. The results for two different input field strengths in the umbral model—as examples—are displayed in Table 2. In the cases presented, much of the trade-off occurs between inferred magnetic field strength and $\eta_0$. The quality of the fits is represented by $\chi^2$ in the last column of the table. Note that $\chi^2$ is smaller (i.e., a better fit) when $B$, $\psi$, and $\phi$ are free parameters. Similarly, Lites & Skumanich (1988) found smaller values of $\chi^2$ for the Mg I lines when both $B$ and $\Delta\lambda_D$ were allowed to be free, as opposed to the case where $B$ was fixed to the "real" value. The small deviations experienced here in Table 2 for the Fe I lines are apparently amplified for the more difficult problem presented by inversion of chromospheric Stokes line profiles.

The temperature stratification is normally retrieved by the SIR inversion to good accuracy (as demonstrated in earlier papers on this method; see references in the introduction). Usually, the differences between the SIR results and the input models are small, less than 50 K from $\log \tau_5 = 0.5$ through $\log \tau_5 = -3.0$, independent of whether $B$, $\psi$, and $\phi$ are allowed to be free parameters. Some other examples of the fits to the temperature stratification are also given below. The improved thermodynamic representation provided by SIR is the reason for the significant reduction in trade-offs as compared to the corresponding ME fitting. The SIR method is apparently able to resolve a well-known trade-off among thermodynamic parameters encountered in the inversion of observed umbral Stokes spectra, as will be discussed in § 5.

### 3.1. *Interpretation of the Line Formation Parameters from ME Inversion*

Using recent techniques for interpreting polarized radiative transfer calculations (e.g., Ruiz Cobo & del Toro Iniesta 1994), it is possible to gain some understanding of the significance of the ME estimates of the parameters $\eta_0$, $\Delta\lambda_D$, and $a$. This is particularly germane with regard to the apparent systematic underestimates of $\eta_0$, which in realistic models undergoes a rapid increase from the bottom to the top of the atmosphere. The values of $\eta_0$ retrieved by the ME inversion represent, as we demonstrate below, the very deepest layers of the model atmosphere, i.e., not the region where the lines under study are generally thought to be formed.

By using generalized response functions (Ruiz Cobo & del Toro Iniesta 1994), we interpret the inferred values from ME fitting through the concept of *height of formation for inferred values*, as proposed by Sánchez Almeida et al. (1996). The computed theoretical formation heights turn out to agree very well with the heights in the model where the value of each parameter is equal to that inferred from the code. This is illustrated in Figure 11. The left panels show the actual stratification of $\eta_0$, $\Delta\lambda_D$, and $a$ (*solid lines*) and the generalized response functions (*dashed lines*) for the quiet-Sun thermal model with $B = 1000$ G, $\psi = 60°$, $\phi = 80°$, and a null macroturbulence. The LOS velocity is zero, the microturbulence velocity is 0.6 km s$^{-1}$, and S/N = 1000. Dashed arrows indicate the (theoretical) height of formation for each inferred parameter, and solid arrows show the height at which the actual stratification coincides with the values retrieved from the ME fit. Note that the slight separation between prediction and inference, apparent in the Doppler width panel, corresponds to less than 0.1 pm difference between the two values. *The low values of $\eta_0$ retrieved by ME fitting are not spurious values due to trade-offs with other parameters; they accurately reflect the true formation properties of this parameter.*

This low formation height of the inferred $\eta_0$ can be understood through the explicit analytical expression of the standard response functions (Sánchez Almeida 1992; Ruiz Cobo & del Toro Iniesta 1994).[7] In LTE, for perturbations on every atmospheric parameter $x$, the response function is

[7] The generalized response functions used to compute the formation height are combinations of the "standard" response functions.

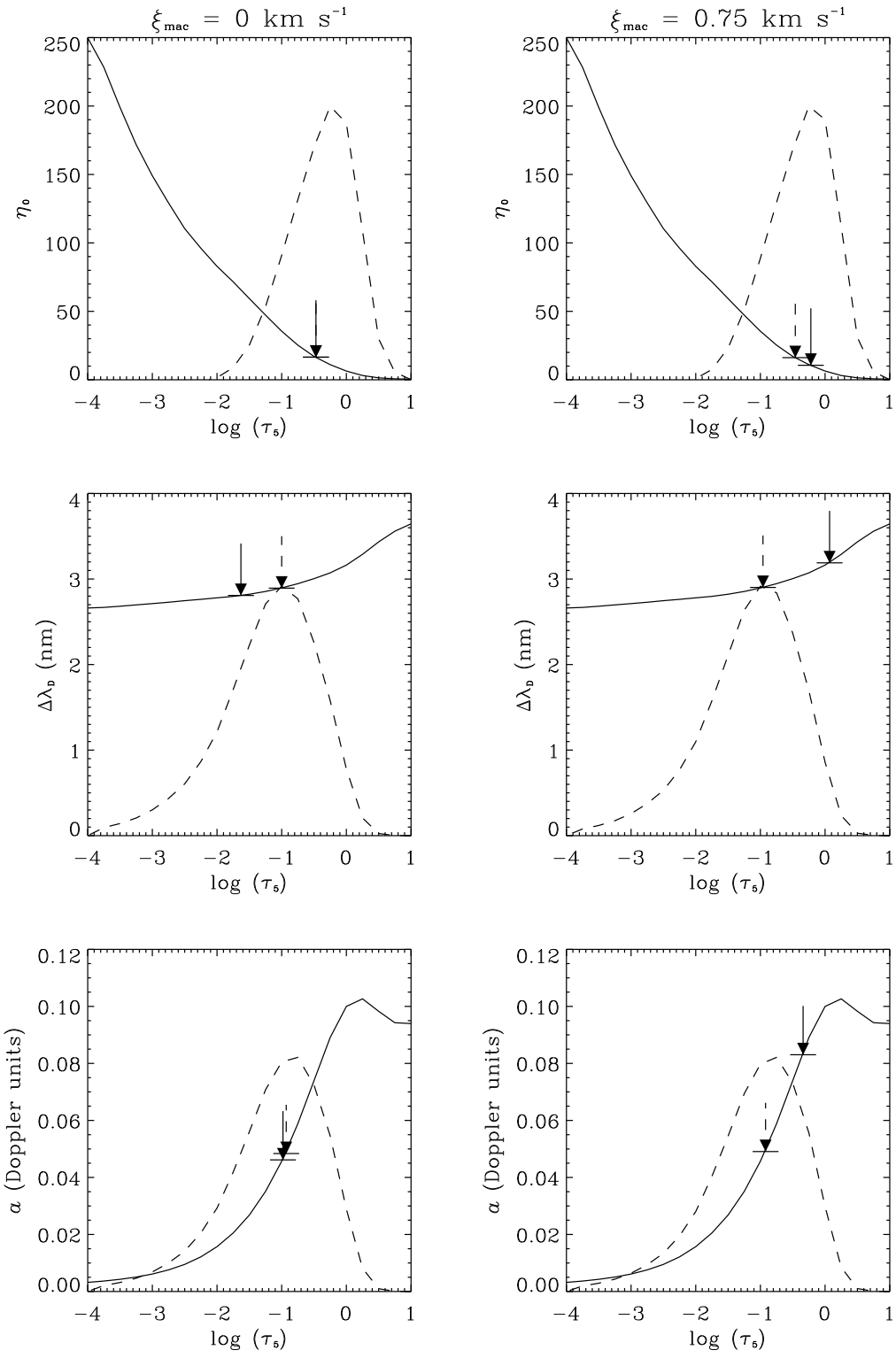


FIG. 11.—Stratification of $\eta_0$, $\Delta\lambda_D$, and $a$ (*solid lines*) and generalized response functions (*dashed lines*) of the ME technique to perturbations in these quantities. Dashed arrows point to the predicted heights of formation, and solid arrows to retrieved ME values. The difference between the two columns is the value of macroturbulence used in the synthetic atmosphere. See text for details.

written as:

$$\boldsymbol{R}_x(\tau_5) = \boldsymbol{O}(0, \tau_5)\left\{\boldsymbol{K}(\tau_5)\,\frac{\partial \boldsymbol{S}(\tau_5)}{\partial x} - \frac{\partial \boldsymbol{K}}{\partial x}\,(\tau_5)[\boldsymbol{I}(\tau_5) - \boldsymbol{S}(\tau_5)]\right\}, \tag{3}$$

where $\boldsymbol{O}$ stands for the evolution operator that appears in the formal solution of the RTE (cf. Landi Degl'Innocenti & Landi Degl'Innocenti 1985), $\boldsymbol{I}$ is the Stokes vector, $\boldsymbol{S}$ is the source function, and $\boldsymbol{K}$ is the "absorption" matrix, which can be expressed as $\boldsymbol{K} = (\kappa_c/\kappa_{c,5})(\mathbf{1} + \eta_0\boldsymbol{\Phi})$ ($\mathbf{1}$ is the $4 \times 4$ identity matrix, $\boldsymbol{\Phi}$ contains the profile shape, and $\kappa_c/\kappa_{c,5}$ is

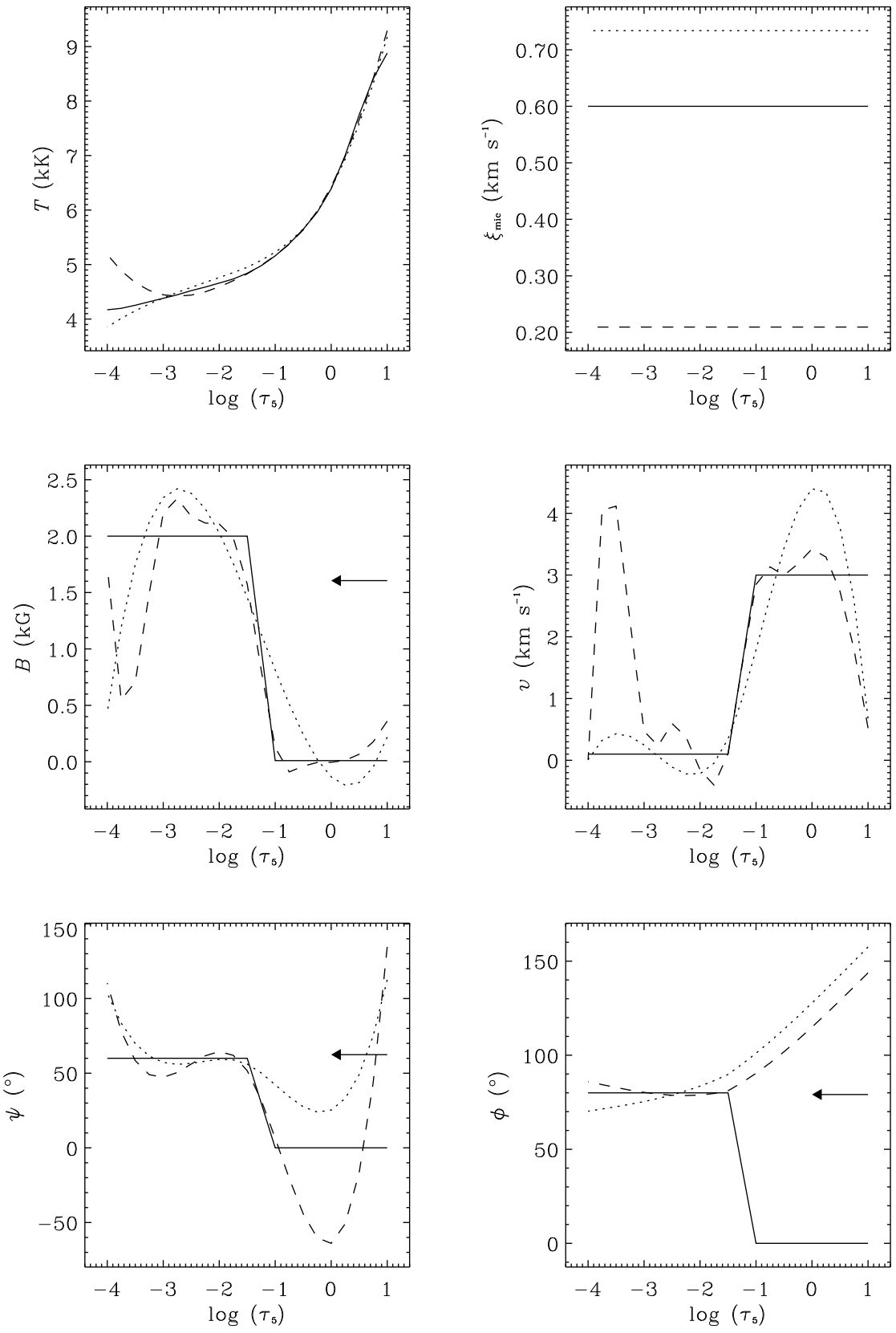


FIG. 12.—Results of the inversion with SIR + 5 (*dotted lines*) and SIR + 11 (*dashed lines*) of Stokes profiles synthesized with a canopy-like variation in the quiet-Sun atmosphere (*solid lines*).

the ratio between the continuum absorption coefficients at the wavelength of the line and at 500 nm). Hence,[8] $\partial \boldsymbol{K}/\partial \eta_0 = (\kappa_c/\kappa_{c,5})\boldsymbol{\Phi}$, i.e., the response function to perturbations on $\eta_0$ does not depend explicitly on $\eta_0$, while the response functions to perturbations on the remaining quantities are proportional to $\eta_0$. Because $\eta_0$ increases rapidly with height, the Stokes profiles are more sensitive to perturbations on the other parameters at higher layers than is the case for perturbations on $\eta_0$.

Another complication may arise in the presence of macroturbulence. A mild macroturbulent velocity does not substantially alter the sensitivity of the Stokes profiles to $\eta_0$, $\Delta\lambda_D$, and $a$, as may be seen by comparing the dashed curves in the left and right columns of panels in Figure 11 (the only difference between columns is the indicated macroturbulence). However, since no explicit macroturbulence parameter is currently included in ME fitting, its effect on the profiles is "sensed" by $\eta_0$, $\Delta\lambda_D$, and $a$. The values of these parameters as derived from the ME inversion change in accordance with an intuitive view of the convolution with a Gaussian-shaped profile: $\eta_0$ decreases (a decrease in the depth of the line) and $\Delta\lambda_D$ and $a$ increase (a broadening of the line). The dashed arrows in the right column are indicators of the theoretical formation heights; i.e., inferred and theoretical values would coincide should the ME inversion consider macroturbulence as a free parameter.

## 4. INFERENCE OF SUPERPENUMBRAL CANOPY STRUCTURE

Canopy-like structures—sharp discontinuities in the stratification of the magnetic field and flows along the LOS—have long been suggested as an explanation for varied observational properties in and around active regions, even in the quiet Sun. Recent observations provide more direct evidence for the presence of such structures in the solar photosphere (see Introduction for references). Taken together, these studies build a very strong case for canopies surrounding sunspots, but since these analyses are based largely on techniques that provide no discrimination of observables along the LOS, some improvement in the diagnostic capability is needed. The SIR inversion provides us with a tool that has the potential to explore canopy structures in a quantitative fashion. However, even the ME inversion is capable of yielding some information on canopy-like structures (Skumanich et al. 1992). In this section, we test the utility of the SIR inversion for extraction of such information from observations.

We have performed SIR inversions of several canopy-like model atmospheres. Here we consider the quiet-Sun thermal model with discontinuities in $B$, $\psi$, and $\phi$ as well as in the LOS velocity (cf. Fig. 12). A $\xi_{mac} = 0.75$ km s$^{-1}$ has been employed. The assumed input stratification is again shown by solid lines. We have examined one inversion with SIR + 5 and another with a larger number of nodes for $B$, $v$, $\psi$, and $\phi$ (11 for $B$ and $v$, five for $\psi$, and three for $\phi$; hereafter referred to as SIR + 11). Increasing the number of nodes results in an increasingly better approach to reproducing the actual discontinuities, as may be seen in Figure 12. The results corresponding to SIR + 5 are plotted in dotted lines, those for SIR + 11 in dashed lines. Note that even SIR + 5 already indicates the presence of a canopy. SIR + 11 provides a good agreement between input and output atmospheres within the $\log \tau_5 = [-3, 0.5]$ range. Obviously, wherever $B = 0$ G, the magnetic inclination and azimuth become irrelevant. In other examples, in which $B$ drops not to 0 but to a significant value, $\psi$ and $\phi$ are well recovered. The results from ME fitting are indicated by arrows.

[8] Note that $\partial \boldsymbol{S}(\tau_5)/\partial \eta_0 = 0$, since $\boldsymbol{S}$ only depends on temperature.

## 5. SUNSPOT STOKES PROFILES

In this section, we present results of analysis of a few specific points within an ASP map of a sunspot within NOAA region 7197, observed on 1992 June 18 at $\mu = 0.96$. We refer the reader to Skumanich et al. (1994), where some ME results are discussed, for specific details of the observations of this sunspot. A thorough SIR analysis of the full two-dimensional ASP map is deferred to subsequent papers of this series.

Three profiles, corresponding to the umbra, the penumbra, and just beyond the outer penumbral boundary, are considered here. These points have been selected to represent three distinct zones of the spot where clearly different stratifications of the various physical quantities must occur. The Stokes profiles are plotted in Figures 13, 14, and 15 along with corresponding ME fitting and SIR + 5 fits to the data (dots represent data, lines represent fit). The ME fits to the data have been shifted downward to clarify the presentation. The ordinates refer only to the SIR fits of the top curves, which are normalized to the mean continuum intensity of the surrounding quiet photosphere. The telluric lines to the red of both Fe I lines are excluded from the fitted regions in both inversion methods. In the case of ME fitting, the far wings of the Fe I lines are also excluded from all Stokes parameters. However, for the SIR inversions, we have used the entire spectral region shown in the $Q$-, $U$-, and $V$-profiles. The far wings of the intensity profile are also fit. Telluric line absorption affects the amplitudes of $Q$, $U$, and $V$ by an amount proportional to the decrease in Stokes $I$, but this effect is usually quite small; with the possible exception of the umbral Stokes $V$-profile, the solar polarization signal lies below the noise level at the wavelengths of these telluric lines. By fitting the entire polarization profiles, we can take advantage of the asymmetry information contained in a comparison of the red and blue wings to help constrain the LOS gradients. The small telluric lines that appear in the $I$-profile fits arise from the presence of a stray-light and/or nonmagnetic (fill factor) contribution fitted by the inversion. Note that the SIR fits are better than the ME fits. The weak asymmetry in the displayed ME profiles arises from an instrumental effect that also introduces a weak asymmetry in the data. This effect is accounted for in both inversion schemes, as the data are not corrected for it. Note that the plots are extended beyond the fit domain.

The inferred SIR + 5 model atmospheres for the umbra (*solid lines*), penumbra (*dash-dotted lines*) and sunspot close environs (*dashed lines*) are plotted together in Figure 16. In the calculations, the models extend from $\log \tau_5 = 1$ to $-4.04$. Layers not shown in the plots correspond to optical depths for which the spectral lines carry negligible information, i.e., that have response functions close to zero. Hence, $T$ is displayed down to $\log \tau_5 = 0.37$, while the remaining quantities are only shown to $\log \tau_5 = 0$ (see Ruiz Cobo & del Toro Iniesta 1992, 1994). Error bars represent formal standard errors for the different nodal quantities. The vector magnetic field is given in the observer coordinate

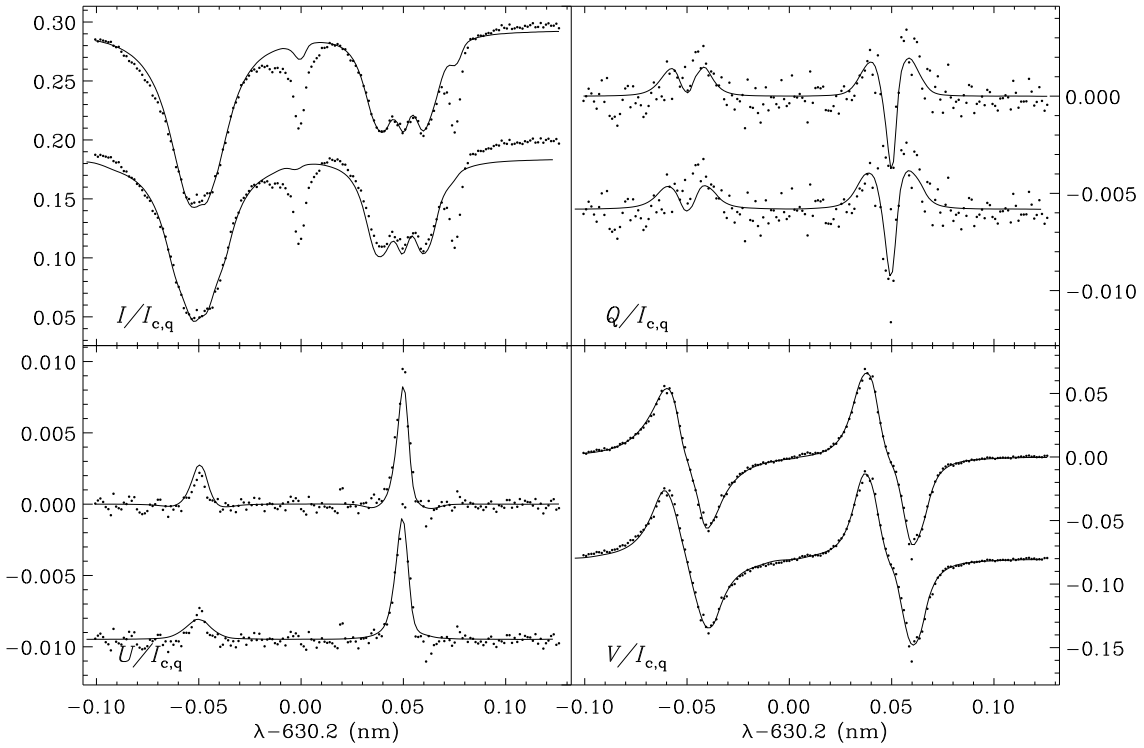


FIG. 13.—Umbral Stokes profiles observed with the ASP (*dots*) and fits from SIR (*upper row*) and ME fitting (*lower row*; shifted downward arbitrarily)

frame. The results from ME fitting are shown with arrows in the $B$, $\psi$, and $\phi$ panels of the figure.

The temperatures of the umbral point fall in between those of the hot and cool models of Collados et al. (1994). The microturbulence velocity is fixed to zero in the SIR model, following the results of those authors for their cool umbral model. The LOS variation of the field strength in the photosphere from the SIR inversion is larger than that of the models cited. Between $\log \tau_5 = 0$ and $-2.75$, $\Delta B \approx 1200$ G, i.e., a rough mean gradient of 4 G km$^{-1}$. This value might be somewhat striking in view of former estimates of the gradient (see Collados et al. 1994 and refer-

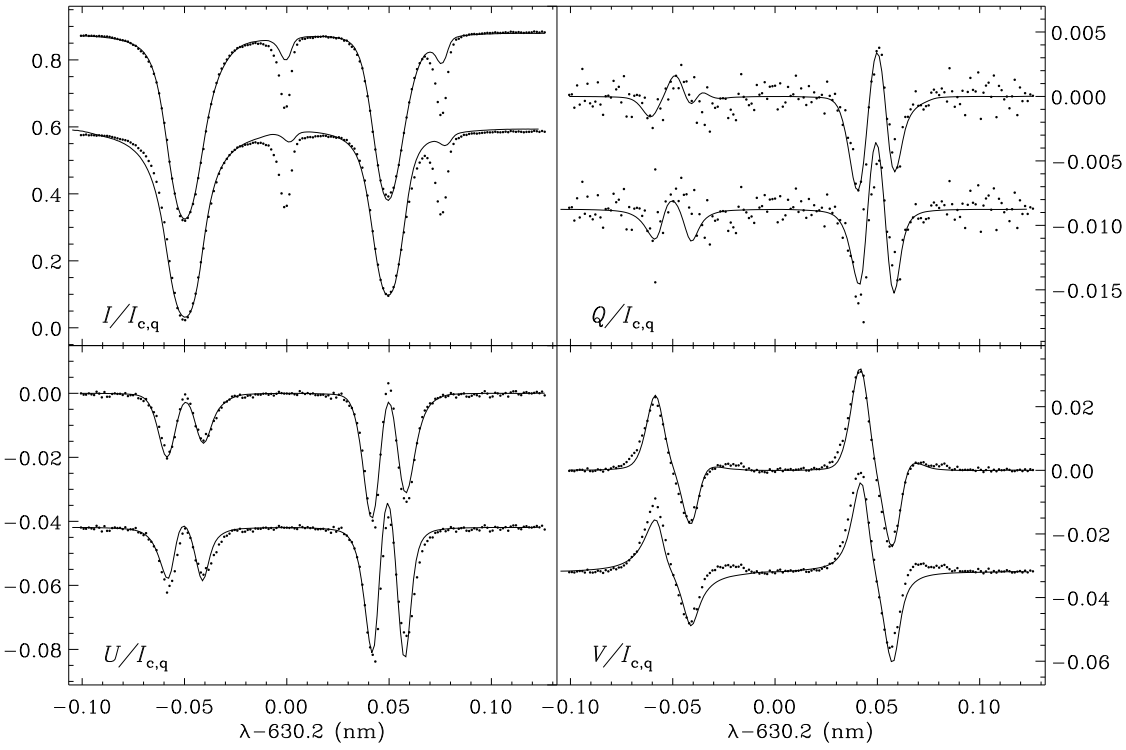


FIG. 14.—Same as Fig. 13, for a penumbral point

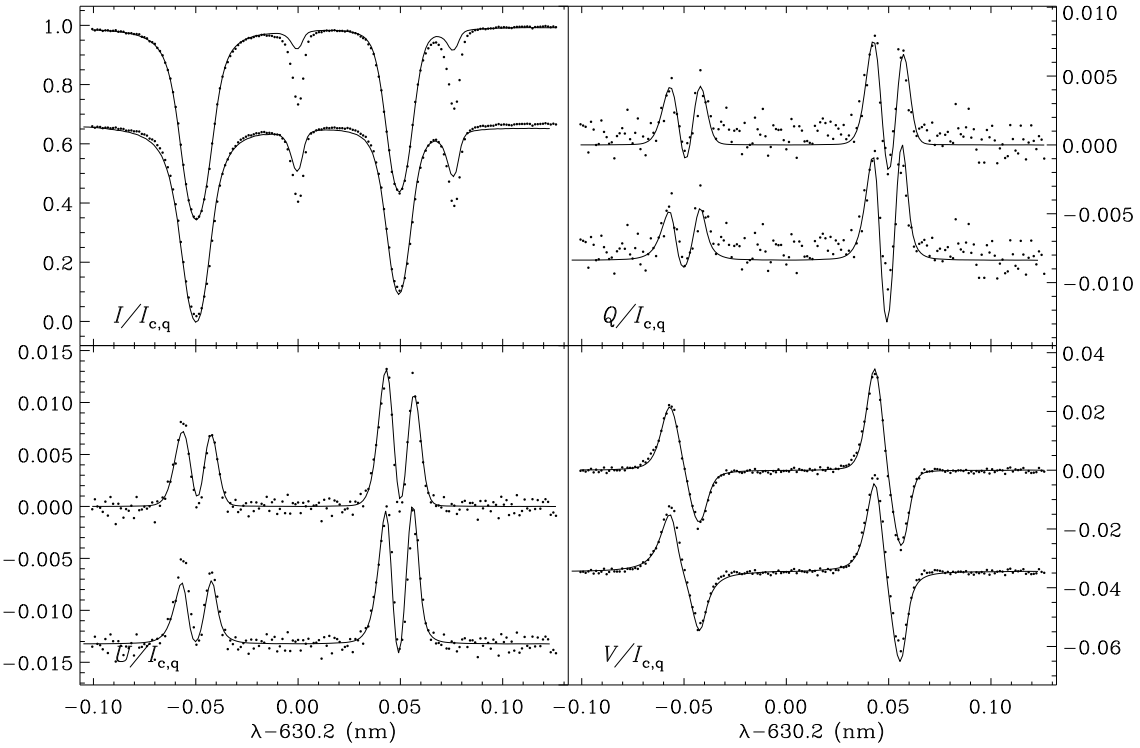


FIG. 15.—Same as Fig. 13, for a point close to the continuum penumbral boundary

ences therein). However, no general conclusions about umbral fields can be drawn from this single point, and we defer a full discussion to the next paper of this series. A slight gradient in inclination is also present in the fit. Note that the angles shown are consistent with the field being nearly vertical (because $\cos\theta = 0.96$). The LOS velocity is consistent with an umbra at rest throughout the entire photosphere (we use an absolute wavelength calibration; see Martínez Pillet, Lites, & Skumanich 1997 for details).

The umbral Doppler width resulting from the SIR + 5 inversions yields $2.2 \lesssim \Delta\lambda_D \lesssim 2.5$ pm, a reasonable value for the umbra of a sunspot where most of the broadening is thermal. The SIR method apparently resolves a well-known problem of the ME inversion code in dealing with the thermodynamic parameters extracted from umbral observations; when umbral Stokes profiles are fitted with ME models allowing free variation of $\Delta\lambda_D$, line damping $a$, and $\eta_0$, unphysically small values of $\Delta\lambda_D$ are often encountered (Skumanich & Lites 1987). This is a trade-off mainly among the thermodynamic parameters; the vector field quantities are only slightly affected because within umbrae the fully split Zeeman components accurately specify the vector field to a reasonable degree of independence of precise values of $\Delta\lambda_D$, $a$, and $\eta_0$. The "fix" usually applied to ME procedures is to invoke a lower limit to the allowed range of the Doppler width, usually the thermal width of the line in question at temperatures typical of the umbral photosphere. If we allow the ME inversion to seek the optimal (in the least-squares sense) parameters for the umbral profiles of Figure 13, we find that $\Delta\lambda_D$ decreases from 2.0 to 1.3 pm, $a$ increases from 0.73 to 1.18, and $\eta_0$ increases from 20 to 29. The SIR procedure apparently resolves this long-standing source of trade-off among thermodynamic parameters arising from ME inversions.

Compared to the mean penumbral model of del Toro Iniesta et al. (1994), the inferred penumbral temperatures are cooler in deep layers and nearly the same in upper layers. Note that the field strength increases and the inclination decreases with height. The ME fit ($\approx$700 G) coincides roughly with $B(\log\tau_5 = -1.5)$. Beyond this point a significant gradient in field strength occurs, with $B \simeq 1900$ G at $\log\tau_5 = -3$. In the deepest penumbral layers, the field is approximately perpendicular to the LOS, which at this disk position indicates a field pointing into the surface! However, the inclination with respect to the LOS at the uppermost layers is on the order of $\psi \simeq 60°$. This is an interesting new result from the SIR analysis, as recent observational studies regarding the inclination of $\boldsymbol{B}$ at the edge of the penumbra-quiet photosphere border (where this particular point is located) indicate the spatially averaged vector field to be inclined by 70°–80° (e.g., Lites & Skumanich 1990; Title et al. 1993; Skumanich et al. 1994). A "fluting" of the penumbral field, where the inclination of the field fluctuates as a function of azimuthal angle about the center of a sunspot, has been at least partially resolved spatially (see review by Lites 1997 and references therein). Although the penumbral field is often observed at high resolution to approach the horizontal in these flutes, instances of the vertical component having an opposite sign to that of the bulk of the sunspot are almost never seen. This suggests that previous techniques are relatively insensitive to $\boldsymbol{B}$ at such deep layers, as verified by the ME inversions of these data indicated in Figure 16. The LOS velocity stratification of this penumbral point is also interesting. On the one hand, significant gradients are apparent. Note that the existence of large velocity gradients have already been reported (e.g., Sánchez Almeida & Lites 1992; del Toro et al. 1994). On the other hand, redshifted velocities appear at the

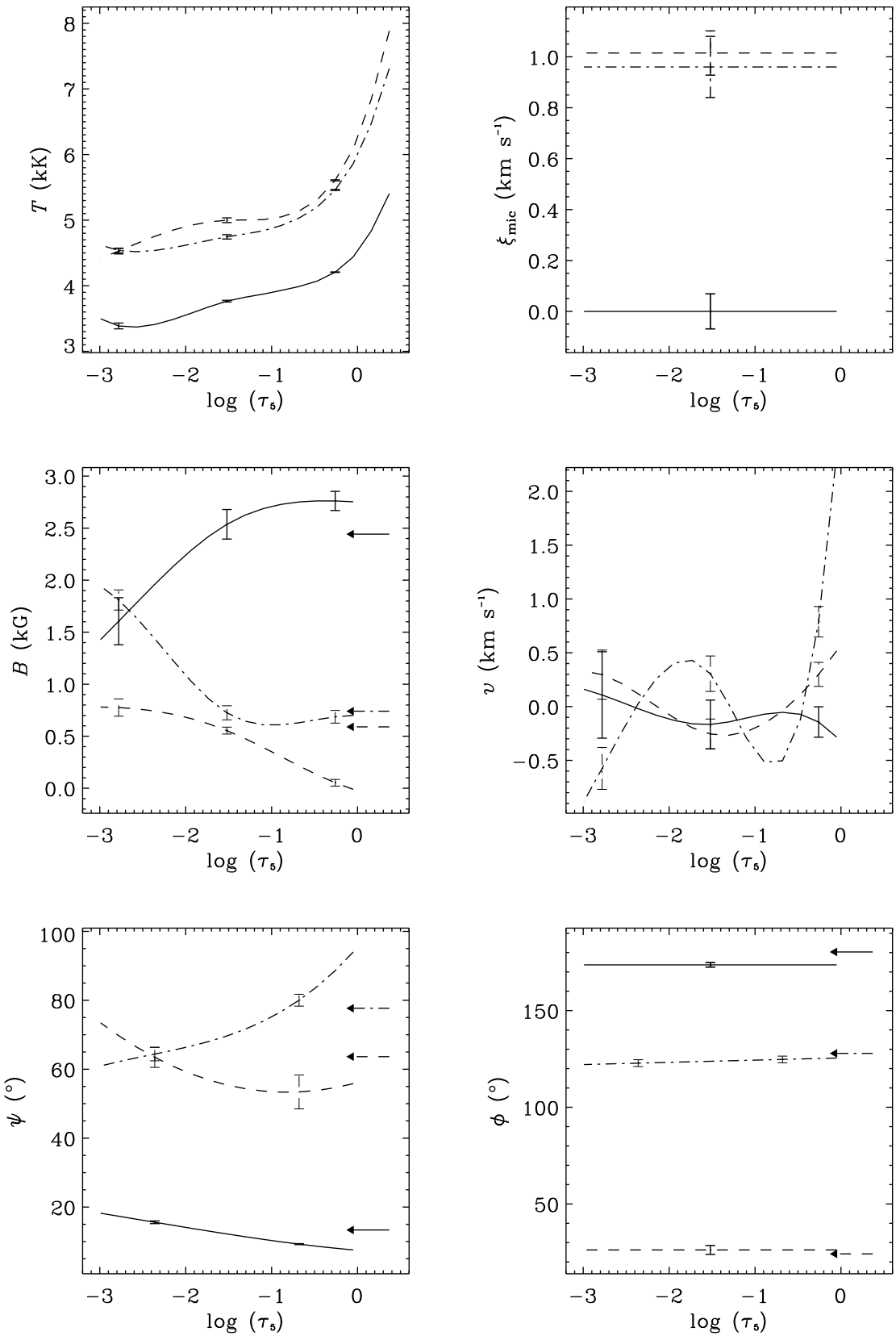


FIG. 16.—Resulting model atmospheres from SIR corresponding to the fits of Figs. 13, 14, and 15. Umbra is represented by solid line, penumbra by dash-dotted line, and the canopy by a dashed line. Results for $B$, $\psi$, and $\phi$ from ME fitting are shown by arrows.

deepest layers, while blueshifted velocities are present at the highest layers. Again, this is a single point, but preliminary results from other regions of the spot indicate that this penumbral stratification is not atypical. A detailed discussion of whether this stratification is really solar or a consequence of numerical effects is deferred to further papers of this series. We must note that our thermal fit (in accordance with any other extant penumbral model) is predicated on hydrostatic equilibrium along the LOS, while one expects such equilibrium along field lines. However, the slight dependence of Fe I lines on electronic pressure (e.g., Gray 1992) suggests that errors are not too large (mainly for the vector magnetic field stratification).

Perhaps the most exciting results of this paper are those derived for the point located just beyond the penumbral boundary. Here, the temperatures are 200–300 K higher than in the penumbra, and the microturbulence is essentially unchanged. Although the field strength increases with height as for the penumbral point, the stratification is completely different; $B \approx 0$ G around $\log \tau_5 = 0$ and nearly constant for $\log \tau_5 \in [-3, -2]$, where the field is inclined with respect to the LOS (but not by more than 70°). This result is clear, direct evidence for the existence of a superpenumbral canopy, as suggested by the other studies of photospheric fields cited above, and indeed also by H$\alpha$ observations. Note that the transition between the nonmagnetic and the magnetic zone looks very smooth and that no sharp boundary is apparent. We believe this result to be valid, because SIR + 11 (see § 4) produces no significant change to the SIR + 5 fit.

## 6. CONCLUSIONS

The principal conclusions of this work may be summarized as follows:

1. Contrary to prior expectations, the ME inversion applied to Stokes profile observations of lines in the visible spectrum can distinguish field strengths as small as 100–200 G, provided that the filling factor is unity. The SIR inversion, having a more detailed representation of the thermal structure and the other line formation parameters, yields even more accurate results at these low field strengths.

2. If the observations have an admixture of unpolarized light (due to scattered light and/or a nonmagnetic contribution due to incomplete spatial resolution), both ME fitting and SIR can recover to reasonable accuracy both the vector field and the filling factor, provided that the Stokes profiles remain significantly above the noise level. Therefore, it is still possible with existing spectropolarimeters operating on visible spectrum lines to *detect* weak fields having filling factors significantly less than unity.

3. When compared to SIR + 1, the ME technique does not usually make serious errors in the LOS-averaged vector field, as a result of both its crude approximation to the depth variation of the source function and the constancy of the line formation parameters $\eta_0$, $\Delta\lambda_D$, and $a$. The SIR + 1 inversions, which like the ME inversions hold field vector and velocity parameters constant through the atmosphere, yield smaller errors in these quantities relative to the ME results, largely as a result of their higher order description of the temperature structure, which also permit us to retrieve the temperature stratification to high accuracy.

4. For the ME fitting and SIR + 1 inversions, which assume a constant field along the LOS, the inferred values for the field strength and the field inclination to the LOS may reflect actual values in the atmosphere at different heights, separated by up to one scale height.

5. The simplicity of the Milne-Eddington approach as compared to a detailed treatment of the radiative transfer, which also recovers accurate thermodynamic information, makes ME fitting far superior in computing speed to SIR + 1; hence, it is recommended for inference of LOS-averaged vector magnetic fields over extended solar regions.

6. In the presence of gradients in the LOS velocity, an inherent redundancy of the Stokes profiles is broken, with the consequence that asymmetric Stokes profiles can convey more information about the atmospheric structure than those arising from a uniformly moving atmosphere. We have confirmed that these gradients are retrieved by SIR inversion.

7. For observations having a S/N = 1000 (i.e., appropriate to modern spectropolarimetric observations relative to the continuum intensity), the Stokes profiles contain sufficient detail to allow one to recover information about variations with optical depth of significantly higher order than linear, as witnessed by the comparison of SIR + 2 and SIR + 5 results.

8. Choosing the appropriate number of nodes to be used by SIR for inverting a particular family of real Stokes profiles is not trivial, and often implies some interactive adjustment. In the future, we expect to enhance the SIR procedure so that it can dynamically adjust the number of nodes for specified parameters, in order to optimize the fit.

9. The ME technique can experience trade-offs among the various parameters, such as the source function, $\eta_0$, $\Delta\lambda_D$, and $a$, and to a lesser extent, trade-offs between these parameters and the vector field. Such trade-offs are significantly reduced with higher order representations of the atmosphere by SIR. We have demonstrated that SIR is able to overcome the long-standing trade-off of the ME inversion among $\eta_0$, $\Delta\lambda_D$, and $a$.

10. The Milne-Eddington line formation parameters $\eta_0$, $\Delta\lambda_D$, and $a$ retrieved by ME fitting can be understood in the light of radiative transfer through the concept of height of formation for inferred parameters.

11. The SIR inversion may recover even rather sharp LOS discontinuities in the magnetic field parameters, as are suspected to occur in magnetic canopies. If very high spatial resolution observations of Stokes profiles become available in the future, we expect that it will be possible to quantify canopies surrounding individual flux tubes using the inversion techniques described here. This would be of great interest in investigating the dynamics of these small elements and their possible influence on the heating of the upper atmospheric layers.

12. The ME and SIR inversion schemes have been applied to real ASP observations of three spatial points within and just outside of a sunspot. The umbral point indicates a rather large gradient of field strength with height. The point near the outer edge of the penumbra indicates a field that changes polarity at deep layers. The point just outside of the sunspot (in the canopy) shows a gradual increase of field strength above the photosphere rather than an abrupt one.

During the last few years, evidence has been accumulating that supports inversion techniques as the best interpretative tools for spectropolarimetry in particular and for

solar physics in general. In this paper, we have presented further quantitative arguments in their favor. Nowadays, available workstations make application easy and practicable at reasonable computing times. The SIR technique proves to be a significant step forward with respect to the very useful ME fitting, the results of which can be used as initialization for SIR. Based on the philosophy of using ME fitting and then SIR, a complete and detailed tomographic analysis of a whole sunspot will be presented in subsequent papers of this series.

## REFERENCES


Adams, M., Solanki, S. K., Hagyard, M., & Moore, R. L. 1993, Sol. Phys., 148, 201
Auer, L. H., & Heasley, J. N. 1978, A&A, 64, 67
Bellot Rubio, L. R., Ruiz Cobo, B., & Collados, M. 1997, ApJ, 478, L45
Collados, M., Martínez Pillet, V., Ruiz Cobo, B., del Toro Iniesta, J. C., & Vázquez, M. 1994, A&A, 291, 622
Degenhardt, D., & Lites, B. W. 1993a, ApJ, 404, 383
———. 1993b, ApJ, 416, 875
del Toro Iniesta, J. C. 1997, in Trans. IAU A, 23, in press
del Toro Iniesta, J. C., & Ruiz Cobo, B. 1995, in La Polarimétrie, Outil pour L'étude de L'activité Magnétique Solaire et Stellaire, ed. N. Mein & S. Sahal-Bréchot (Paris: Observatoire de Paris), 127
———. 1996, Sol. Phys., 164, 169
———. 1997, in Forum THEMIS, ed. N. Mein & S. Sahal-Bréchot (Paris: Observatoire de Paris), in press
del Toro Iniesta, J. C., Tarbell, T. D., & Ruiz Cobo, B. 1994, ApJ, 436, 400
Elmore, D. F., et al. 1992, Proc. SPIE, 1746, 22
Gingerich, O., Noyes, R. W., Kalkofen, W., & Cuny, Y. 1971, Sol. Phys., 18, 347
Giovanelli, R. G., & Jones, H. P. 1982, Sol. Phys., 71, 5
Gray, D. F. 1992, The Observation and Analysis of Stellar Photospheres (2d ed.; Cambridge: Cambridge Univ. Press)
Jefferies, J., Lites, B. W., & Skumanich, A. 1989, ApJ, 343, 920
Kjeldseth-Moe, O., & Maltby, P. 1974, Sol. Phys., 97, 239
Landi Degl'Innocenti, E., & Landi Degl'Innocenti, M. 1981, Nuovo Cimento, 62B, 1
———. 1985, Sol. Phys., 97, 239
Lites, B. W. 1997, Trans. IAU A, 23, in press
Lites, B. W., Elmore, D. F., Seagraves, P., & Skumanich, A. P. 1993, ApJ, 418, 928
Lites, B. W., Leka, K. D., Skumanich, A., Martínez Pillet, V., & Shimizu, T. 1996, ApJ, 460, 1019
Lites, B. W., Martínez Pillet, V., & Skumanich, A. 1994, Sol. Phys., 155, 1
Lites, B. W., & Skumanich, A. 1988, ApJ, 330, 493
Lites, B. W., & Skumanich, A. 1990, ApJ, 348, 747
Maltby, P., Avrett, E. H., Carlsson, M., Kjeldseth-Moe, O., Kurucz, R. L., & Loeser, R. 1986, A&A, 306, 284
Martínez Pillet, V., Lites, B. W., & Skumanich, A. 1997, ApJ, 474, 810
Rachkovsky, D. N. 1962, Izv. Krymskoi Astrofiz. Obs., 27, 148
———. 1967, Izv. Krymskoi Astrofiz. Obs., 37, 56
Rimmele, T. R. 1995a, A&A, 298, 260
———. 1995b, ApJ, 445, 511
Ruiz Cobo, B., & del Toro Iniesta, J. C. 1992, ApJ, 398, 375
———. 1994, A&A, 283, 129
Ruiz Cobo, B., del Toro Iniesta, J. C., Rodríguez Hidalgo, I., Collados, M., & Sánchez Almeida, J. C. 1996, in ASP Conf. Ser., Cool Stars, Stellar Systems, and the Sun, ed. R. Palavicini & A. K. Dupree (San Francisco: ASP), in press
Ruiz Cobo, B., Rodríguez Hidalgo, I., & Collados, M. 1997, ApJ, in press
Sánchez Almeida, J. 1992, Sol. Phys., 137, 1
Sánchez Almeida, J., & Lites, B. W. 1992, ApJ, 398, 359
Sánchez Almeida, J., Ruiz Cobo, B., & del Toro Iniesta, J. C. 1996, A&A, 314, 295
Skumanich, A., Grossmann-Doerth, U., & Lites, B. W. 1992, in Methods for the Determination of Solar and Stellar Magnetic Fields, ed. M. Faurobert-Scholl, H. Frisch, & N. Mein (Meudon: Observatoire de Meudon), 57
Skumanich, A., & Lites, B. W. 1987, ApJ, 322, 473
Skumanich, A., Lites, B. W., & Martínez Pillet, V. 1994, in ASI Ser. 433, Solar Surface Magnetism, ed. R. J. Rutten, & C. J. Schrijver (New York: NATO), 99
Solanki, S. K., Finsterle, W., & Rüedi, I. 1996, Sol. Phys., 164, 253
Solanki, S. K., Montavon, C. A. P., & Livingston, W. 1994, A&A, 283, 221
Solanki, S. K., Rüedi, I., & Livingston, W. 1992, A&A, 263, 339
Stanchfield, D. C. H., Thomas, J. H., & Lites, B. W. 1997, ApJ, 477, 485
Title, A. M., Frank, Z. A., Shine, R. A., Tarbell, T. D., Topka, K. P., Scharmer, G. B., & Schmidt, W. 1993, ApJ, 393, 782
Zhang, H. 1994, Sol. Phys., 154, 207